Diffusion-Weighted Imaging Outside the Brain: Consensus Statement From an ISMRM-Sponsored Workshop

Bachir Taouli, MD[1,*], **Ambros J. Beer, MD**[2], **Thomas Chenevert, PhD**[3], **David Collins, BA**[4], **Constance Lehman, MD, PhD**[5], **Celso Matos, MD**[6], **Anwar R. Padhani, MD**[7], **Andrew B. Rosenkrantz, MD**[8], **Amita Shukla-Dave, PhD**[9], **Eric Sigmund, PhD**[10], **Lawrence Tanenbaum, MD**[11], **Harriet Thoeny, MD**[12], **Isabelle Thomassin-Naggara, MD, PhD**[13], **Sebastiano Barbieri, PhD**[12], **Idoia Corcuera-Solano, MD**[1], **Matthew Orton, PhD**[4], **Savannah C. Partridge, PhD**[14], and **Dow-Mu Koh, MD**[15]

[1]Department of Radiology and Translational and Molecular Imaging Institute, Icahn School of Medicine at Mount Sinai, New York, New York, USA [2]Department of Nuclear Medicine, University Hospital Ulm, Ulm, Germany [3]Department of Radiology, University of Michigan, Ann Arbor, Michigan, USA [4]CR UK Cancer Imaging Centre, Institute of Cancer Research and Department of Radiology, Royal Marsden Hospital, London, UK [5]Department of Radiology, Massachusetts General Hospital, Boston, Massachusetts, USA [6]Department of Radiology, Champalimaud Clinical Centre, Lisbon, Portugal [7]Mount Vernon Cancer Centre, Northwood, UK [8]Department of Radiology, NYU Langone Medical Center, New York, New York, USA [9]Departments of Medical Physics and Radiology, Memorial Sloan-Kettering Cancer Center, New York, New York, USA [10]Irene and Bernard Schwartz Center for Biomedical Imaging (CBI) and Center for Advanced Imaging and Innovation (CAI2R), Department of Radiology, NYU Langone Medical Center, New York, New York, USA [11]Department of Radiology, Icahn School of Medicine at Mount Sinai, New York, New York, USA [12]Department of Diagnostic Radiology, Inselspital Bern, Bern, Switzerland [13]Université Pierre et Marie Curie, Hôpitaux Universitaires Paris-Est, Paris, France [14]Department of Radiology, University of Washington, Seattle, USA [15]Institute of Cancer Research and Department of Radiology, Royal Marsden Hospital, London, UK

Abstract

The significant advances in magnetic resonance imaging (MRI) hardware and software, sequence design, and postprocessing methods have made diffusion-weighted imaging (DWI) an important part of body MRI protocols and have fueled extensive research on quantitative diffusion outside the brain, particularly in the oncologic setting. In this review, we summarize the most up-to-date information on DWI acquisition and clinical applications outside the brain, as discussed in an ISMRM-sponsored symposium held in April 2015. We first introduce recent advances in acquisition, processing, and quality control; then review scientific evidence in major organ systems; and finally describe future directions.

*Address reprint requests to: B.T., Icahn School of Medicine at Mount Sinai, Department of Radiology and Translational and Molecular Imaging Institute, 1470 Madison Ave., New York, NY 10029. bachir.taouli@mountsinai.org.

Extracranial diffusion-weighted imaging (DWI) is now widely applied in clinical practice to enhance disease assessment, particularly in the oncological setting. A National Cancer Institute (NCI)-sponsored open consensus meeting was held in 2008 in Toronto during the ISMRM meeting, which led to the publication of a consensus and recommendation article in 2009.[1] Since then, the field of body DWI has seen rapid expansion in both research and clinical applications. In 2015, an ISMRM-sponsored meeting was held from the 1st to 3rd April in Boston, which aimed to survey the current state-of-the-art knowledge and developments in extracranial DWI. This article summarizes the discussions and consensus opinions at that meeting, and provides a broad review and update of developments in the field.

Recent Technological Advances in DWI Acquisition

DWI is increasingly finding powerful applications outside the brain, where it was first used. This migration has been enabled by several factors, including technological advances, pulse sequence development, and new data analysis frameworks.

DWI in clinical scanners is generally performed with single-shot k-space trajectories, most commonly the echoplanar imaging (EPI), and analysis is performed on the magnitude channel, discarding the phase information. Single-shot EPI collects a series of gradient echoes to fill in the required k-space raster. Since the resulting echo train occurs over a finite time interval, they suffer 1) phase shifts and 2) signal attenuation from variations in the local applied magnetic field. These effects can be reduced by shortening the echo train length (ETL), by increasing receiver bandwidth, or using undersampling from partial Fourier reconstruction,[2] multiple receiver coil parallel imaging,[3] or both. Higher gradient systems have thus shortened readouts and improved EPI DWI. Higher field strength systems present competing influences for DWI (higher signal-to-noise ratio [SNR] vs. shorter relaxation times, etc.) but eventually successful compromises have been achieved. For example, RF field (B1) inhomogeneity at higher field can be particularly pronounced for large abdominal fields of view (FOVs), but the rise in prevalence of receiver array coils allowed a reversal of this disadvantage by enabling better parallel imaging performance. Image-based shimming[4] has also been applied to emphasize the image quality of target areas within a large FOV. Similarly, transmit fields have been controlled to a higher degree to benefit DWI. Given the large fields of view and image matrices for body imaging, an increasingly prevalent approach is to limit the imaged volume to a target zone (reduced field of view, rFOV) (Fig. 1) either by inner volume imaging (IVI) or outer volume suppression (OVS). This approach has found application in thyroid,[5] pancreas,[6] kidney,[7] breast,[8,9] and spinal cord[10] DWI. Multiple excitation body coils, making selective excitation via shaped RF pulses more feasible with shorter pulse durations in the context of parallel transmission, have been demonstrated.[11]

Multishot DW EPI sequences using 2D navigators have been successfully applied in the brain, although more severe motions limit use in the abdomen. Alternative to EPI readout, a train of RF pulses in turbo spin echo / fast spin echo (TSE/FSE) sequences "undo" phase evolution, thereby effectively removing spatial distortion. While TSE/FSE is extremely robust and widely used for traditional imaging, insertion of DW gradient pulses in a

TSE/FSE sequence makes the phase of transverse magnetization ill-defined relative to RF-pulse phase. This can lead to substantial artifact in multishot DW TSE/FSE. Fortunately, phase-cycling RF pulses stabilize echo signal amplitude relative to arbitrary initial transverse magnetization phase, thus greatly reduces these artifacts. Strategies to parse *k*-space and incorporate navigator information are varied and include periodically rotated overlapping parallel lines (PROPELLER) via short or long readouts,[12] split-echo propeller (SPLICE), and self-navigated interleaved spirals (SNAILS).[13–15] The trade-off between low distortion vs. motion artifact immunity for applications such as lesion detection and ADC quantification are being studied. Commercialized versions of these non-EPI-based and multishot techniques are now available and look particularly promising in less kinetic organs such as breast and prostate.[16–18]

For a successful multi-b value DWI experiment, it is important to optimize SNR at each b-value. The number of signal averages is usually increased for higher b values so that a DWI with multiple b-values experiment can be performed at an acceptable SNR in clinically reasonable times.

Another less commonly tuned encoding parameter is the diffusion time. To put it in context, the confinement length scales of extracranial organs often differs from those prevalent in cerebral tissue (~1–10 μm) and DTI (diffusion tensor imaging) metrics are correspondingly different. A useful guide to the diffusion sensitivity is the ratio of the diffusion length to the confinement length scale. When the primary cell size (tubule, myofiber, duct) is larger in scale than cerebral axons, diffusivities are larger and anisotropies are smaller. This drop in contrast can be ameliorated by increasing the diffusion time, which is most conveniently done with a stimulated echo preparation.[19–21] When properly included, this not only increases contrast but detailed tissue modeling can also be achieved at longer diffusion times.[22,23]

In summary, advances in hardware, pulse sequence variations, and generalized analysis have spurred tremendous recent progress in DWI outside the brain. The result is no longer a direct transposition of DWI methods from the brain but an adaptation specific to the challenges and opportunities of extracranial anatomies.

Diffusion Measurement Reproducibility and Precision Assessment

"Repeatability" and "reproducibility" are often used to empirically assess (in)consistency of quantitative measures. In terms of ADC, repeatability relates to the consistency of ADC values when the same imaging test of the same object (patient) is performed at short intervals on the same scanner by the same operator, whereas reproducibility is the consistency of ADC values when the same imaging test (or as close as possible) of the same object is performed on different equipment, typically by different operators at different centers.

Sources of Variance

Performing an ADC estimate spans multiple domains that independently contribute to variance: 1) biological (patient size/shape/cooperativeness/lesion location and heterogeneity/

phenotype; potential therapeutic effects); 2) scan operator (protocol build, patient set-up, skill level); 3) MRI system (hardware/software platform; DWI sequence and acquisition parameters; and individual scanner idiosyncrasies); 4) algorithm to convert DWI to ADC; and 5) radiologist/analyst definition of measurement region.

Technical Variance

The MRI system itself and platform capabilities are the heart of technical variance. Cross-vendor/platform capabilities also lead to protocol variance. While high-level parameters (eg, geometry and b-values) can usually be matched, secondary parameters (DWI waveform design, echo-spacing, shim and fat-suppression technique, etc.) are often difficult to replicate across platforms. Unfortunately, what is the optimal protocol on one platform may not be optimal on another. Physical phantoms offer the best means to assess technical performance. A variety of ADC phantom designs have been proposed.[24,25] Ice-water-based phantoms are popular for multicenter trials since they are inexpensive and provide an absolute truth diffusion coefficient since the media temperature is controlled that would otherwise add large uncertainty (>10%) in ADC values. In one phantom study across 35 multivendor/field-strength/site MRI systems, intraexam stability of ice-water ADC measured at magnet isocenter was ~1% (2SD/Mean). Longer-term repeatability and cross-system reproducibility (34 systems excluding one outlier) were comparable at ~4% (2SD/Mean) at isocenter,[26] although increased systematically for off-center ADC,[27] with mean ADC bias estimated in vitro at −20% (±20%, superior–inferior) and +7% (±15%, right–left) for measurements away from isocenter.[27] The ~4% reproducibility represents a technical baseline level to which other sources (biology, analysis methods) will add. Note that repeatability and interplatform reproducibility in vivo will not be as good as the one for phantoms, due to added complexity during acquisition (motion, cardiac and pulsation artifacts, shimming, fat suppression, etc.). System performance metrics used for site certification and periodic QC (quality control) in multicenter trials include: ADC bias from known value; spatial variation in ADC; intra-exam ADC stability; DWI SNR; and acquisition protocol compliance.

Repeatability and Reproducibility of ADC in Tissues

Since diffusion measurement is completely noninvasive, it can be repeated within a single exam, which is certainly more convenient for patients. Rather than merely acquire two DWI series in immediate succession, the "coffee break" method offers some resemblance to the preferred repeated measures experiment, which spans multiple scan dates. Intravendor and intervendor variance of brain ADC was studied using 12 human phantoms each scanned at different institutions, as well as repeated scans on two human phantoms on each system.[28] Intraindividual differences from repeated scans on the same system were 2.5–5.4%, whereas the average intervendor differences ranged from 3.8–8.8%. For normal tissues in the abdomen, a short-term and long-term repeatability study on one 3T scanner revealed a 14% coefficient of variation (CV = SD/mean).[29] These results were similar to another abdominal study that also compared various acquisition techniques.[30] In abdominal tumors, a two-site reproducibility study in 16 patients revealed a 14% coefficient of repeatability (2SD/Mean) for ADC calculated from b-value range 0–750, but much higher value (less consistent) using low b-values 0–100.[31] Another recent study in hepatocellular carcinoma (HCC) reported

poor reproducibility of IVIM parameters D* and PF/f with CVs of 60.6% and 37.3%, while D/ADC had much better reproducibility (CV 19.7% and <16%).[32]

Diffusion Quantification Beyond ADC

For nearly 30 years the ADC has been employed to describe water diffusion within biological tissues. The term "apparent diffusion" was used at the outset of clinical DWI in recognition that biological tissues are heterogeneous and contain multiple interacting compartments. These interactions include, among others, water exchange and blood flow, and these properties will result in non-Gaussian diffusion. However, early diffusion measurement protocols using only two b-values (until recently of modest magnitude [<1000 s/mm^2]) limited the analysis of diffusion data to the simplest model possible that of Gaussian diffusion described by a monoexponential model from which the ADC is estimated.[33] Modern clinical MR scanners benefit from multiple technical advancements in radiofrequency and gradient hardware that have resulted in significant improvements in DWI and there is now the opportunity to employ protocols using multiple b-values including b-values exceeding 2000 s/mm^2 in the body. Using multiple b-values, particularly b-values in the range 0–200 s/mm^2, sensitizes the diffusion measurement to capillary perfusion and other flow phenomena.[34]

Intravoxel Incoherent Motion (IVIM) DWI

IVIM DWI models the diffusion-attenuated MRI signal as a sum of a static tissue molecular diffusion (D: diffusion coefficient, also reported as Dt: true diffusion coefficient, in mm^2/s) and perfusion-related pseudodiffusion: perfusion fraction (PF or f, which reflects the fraction of flowing blood, in %) and pseudodiffusion coefficient (D*, which reflects the velocity of capillary blood, in mm^2/s)[34–36] (Fig. 2). A free-breathing or respiratory-triggered fat-suppressed single-shot (SS) EPI sequence is suggested using a minimum number of b values. Optimal b-value selection for IVIM is more complex than for ADC measurement because there are three parameters related to (in principle) independent tissue properties. There is no clear consensus regarding the optimal number of b values to be used. Recent IVIM studies have used distributions of 5 to 16 b-values that sample both perfusion (≤100 s/mm^2) and diffusion (>100 s/mm^2) regimes.[37–44] Because more b-value samples involve longer scan time, there is a need to use the smallest possible number of b-values where possible, for example, down to 4 b values in the liver (0, 15, 150, and 800 s/mm^2).[42] An added complexity is that b-value selection is also impacted by other properties of the imaging sequence, for example, the flow sensitivity of the gradient profile, and also on the scanner manufacturer and the accuracy of the b-value calculation. DWI data can be analyzed using the least-square method or Bayesian method. Where IVIM measurements are related to a flow phenomena the potential for directionally oriented flow should be considered. This has been reported in the kidney[45] where the anisotropy was observed for the pseudodiffusion coefficient in the medulla, and in muscle[20] where a reformulation of the IVIM model in terms of "partially" incoherent motion was proposed.

Repeatability studies show that IVIM estimation variability in the body may be within acceptable limits for PF or f, but estimates of the pseudodiffusion coefficient D* are subject

to much larger variations.[42,44,46–48] In some applications, PF/f alone is diagnostic, and in such cases current acquisition and parameter estimation methods will be adequate. However, obtaining reliable D* estimates would increase the scope of IVIM examinations due to the potential link between D* and perfusion or other transport effects. While most published repeatability studies focus on estimates from small regions or whole organs, for the approach to be useful in general reliable voxel-wise estimation is important so that parameter maps may be computed for radiological assessment. The variability reported for regions or organs underestimate the errors with voxelwise estimation.

Diffusion Kurtosis Imaging (DKI)

At higher b-values (>1000 s/mm^2) the signal contribution of water from the extracellular space is substantially reduced, making the diffusion measurement more sensitive to restrictive compartments such as the intracellular compartment.[49–51] The DKI model is an advanced mathematical fitting scheme that requires ultra-high b-values, typically of ~2000 s/mm^2, and provides both a diffusion coefficient D_{app} that is corrected to account for such non-Gaussian behavior as well as an additional metric, the apparent kurtosis, K_{app}, reflecting the extent of the non-Gaussianity. These coefficients are computed using the following equation:

$$S_i = S_0 * e^{\left(-b_i * D_{app} + \frac{1}{6} * b_i^2 * D_{app}^2 * K_{app}\right)}$$

K_{app} close to 0 indicates essentially Gaussian diffusion and is anticipated for b-values less than ~1000 s/mm^2 at which the monoexponential fit generally still applies. Greater K_{app} reflects deviation of the tissue's signal decay from the monoexponential fit as a result of non-Gaussian diffusion behavior and generally is observed to a greater extent as the b-value increases beyond ~1000 s/mm^2. The DKI model has been suggested to better reflect microstructural heterogeneity and complexity of tissue, potentially related to the intracellular environment.

Stretched-Exponential Model

The use of alternative non-Gaussian diffusion models includes a stretched-exponential model.[52,53] This diffusion model contains a single additional stretching term, which can be linked to either non-Gaussian diffusion processes or heterogeneity of Gaussian diffusion processes within each voxel. The model has the advantage of describing both Gaussian and non-Gaussian processes depending on the value of the stretching term. The stretching parameter has been shown to be a useful index of regional heterogeneity in glioma and importantly was shown to be independent of applied gradient direction. This model has found broad application over a wide range of b-values and clinical settings.[54,55] Since water molecules diffuse on the order of a few μm during the course of a typical diffusion measurement and image voxels are on the order of a few mm, the diffusion measurement must represent the statistical properties of a distribution of underlying diffusion coefficients which may or may not be Gaussian processes. A direct approach is therefore to model the signal attenuation as a continuous distribution of diffusion coefficients and estimate statistics of the underlying distribution, as was done using a truncated Gaussian distribution.[56] An

alternative approach uses an effective medium theory to express the diffusion signal in terms of higher-order moments of the diffusion propagator, which results in the DKI model.

Given the number of diffusion models available, it is necessary to evaluate which model best describes the data, assuming the data support such a model. Any given model will require more samples (acquisitions at a given b-value) than the number of free model parameters. Although in principle we can hypothesize a biological basis for choosing to employ a particular diffusion measurement protocol and model, this should be confirmed by testing goodness of fit for a number of diffusion models. A further consideration relating to the employment of diffusion models is to determine if they are robust. It is well known that increasing the number of model parameters may improve the overall model fit but this may be at the expense of poor measurement repeatability and result in correlations between model parameters.

Current Scientific Evidence Outside the Brain *Liver DWI*

LIVER DWI ACQUISITION TECHNIQUE

The fat-suppressed SS EPI technique is the most frequently used sequence in the liver. Most DWI studies have been conducted at 1.5T, although there are increasing reports using 3.0T, due to increased availability and higher SNR. DWI of the liver is usually performed prior to contrast material administration, although performing DWI after the administration of gadolinium-based contrast agents (such as gadoxetic acid) does not significantly affect ADC values.[57,58] The shortest possible echo time (TE) is suggested, as well as the use of parallel imaging to improve SNR and decrease distortion. DWI may be performed in breath-hold (BH) or in free-breathing (FB) mode with multiple signal-averaging to reduce the effects of motion or using a respiratory-triggered (RT) acquisition.[59] The choice of FB vs. RT acquisition is still debated for liver DWI, in terms of image quality and parameter reproducibility. The choice depends on time and equipment availability. For the purpose of ADC quantification, it is generally recommended to acquire FB or RT data, so that multiple b values can be acquired (acquisition time between 2–6 min).

CHOICE OF B VALUES

b values used for liver imaging are typically lower than 1000 s/mm^2. Applying a low b value <100 s/mm^2 provides "black blood" images, which improves liver lesion detection and can be used as a substitute for T_2WI (T_2-weighted imaging). Intermediate and high b values (500 s/mm^2) provide diffusion information used for lesion characterization.[60] We do not recommend the use of a b value of zero for ADC quantification (except when IVIM is performed), in order to decrease perfusion contamination. At least two or three b values (for example, b <100, intermediate b value 400–500, and higher b value between 500 to 1000) should be used for clinical purposes. More b values can be used for the purpose of IVIM.

LIVER LESION DETECTION AND CHARACTERIZATION

DWI is considered to be more sensitive than FSE T_2WI for liver lesion detection.[61] The combination of DWI and CE (contrast-enhanced)-T_1WI is the most sensitive for detection of malignant liver lesions, including liver metastases (Fig. 3) or HCC (Fig. 4). A recent meta-

analysis showed no major difference between DWI and CE-T_1WI using either extracellular or liver-specific gadolinium-based contrast agents for the detection of liver metastases.[62] DWI demonstrates variable sensitivity for HCC detection, and the combination of DWI with contrast agents yields the best sensitivity for HCC detection. ADC quantification can be used to characterize liver lesions as cystic/necrotic or solid (Fig. 5). However, ADC alone is deemed insufficient for liver lesion characterization.[61]

DIAGNOSIS OF LIVER FIBROSIS AND CIRRHOSIS

There are data suggesting lower ADC in cirrhosis compared to noncirrhotic liver, and a negative correlation between liver ADC and the stage of liver fibrosis.[63] It has been observed that the diagnostic performance of ADC is lower than that of liver stiffness measured with MR elastography.[64] There is encouraging data on the use of IVIM for diagnosing fibrosis and cirrhosis[38]; however, comparison with other techniques such as elastography is needed.[65]

LIVER TUMOR RESPONSE

ADC has potential value in the evaluation of liver tumor response, with changes in ADC preceding changes in lesion size. Pretreatment ADC may be used to predict response to treatment. More prospective data are needed to determine the value of ADC in predicting clinical outcomes.[59]

Pancreas DWI

MRI has high contrast resolution to detect the majority of pancreatic diseases through changes in T_1/T_2 relaxation and T_1 contrast enhancement. However, these changes might be insufficient to detect or characterize lesions that are of small size or occur in a background of chronic or acute inflammation. DWI provides another image contrast mechanism that may increase the sensitivity and the specificity of MRI of the pancreas.[66] Different approaches might be used for detection and characterization of pancreatic lesions:

- Use of a single low b-value (<100 s/mm^2) instead of fat-suppressed FSE T_2WI to create black blood contrast. This is mainly used for detection of focal pancreatic lesions and focal liver lesions.

- Use of three b-values (for example, 0, 150, and 1000 s/mm^2) to detect focal pancreatic lesions, examine signal changes, and extract ADC to improve characterization.

- Use of a larger range of b values (typically 9–11 b values ranging from 0 to 1000 s/mm^2) in selected patients (because of the large penalty in acquisition time) to improve the discrimination between focal pancreatitis and pancreatic adenocarcinoma by quantifying IVIM parameters.

PANCREATITIS—There is lack of robust data about the role of DWI in pancreatic inflammation. It has been suggested that acute pancreatitis is associated with impeded diffusion and lower ADC compared to normal parenchyma.[66] Recent studies suggest that DWI used in conjunction with T_2WI and MRCP could be powerful for the assessment of

acute pancreatitis,[67] and that DWI may be useful in detecting infection in pancreatic fluid collections.[68] DWI can also be used to detect focal lesions in autoimmune pancreatitis.

PANCREATIC ADENOCARCINOMA—The addition of DWI to conventional MRI helps to increase the sensitivity of MRI for the detection of small pancreatic adenocarcinomas.[69] PF/f extracted from the IVIM technique has a promising role for differentiation of pancreatic adenocarcinoma from mass-forming pancreatitis.[70] However, this strategy is not easy to implement in the clinic because of the long acquisition time and postprocessing challenges.

PANCREATIC NEUROENDOCRINE TUMORS (FIG. 6)—A recent small series comparing MRI to fluoro-2-D-deoxyglucose / positron emission tomography / computed tomography (FDG-PET-CT) for detection of pancreatic neuroendocrine tumors showed improved detection when adding DWI to T_2WI; while ^{68}Ga-DOTATATE PET-CT was more sensitive than MRI for tumor detection.[71] A significant negative correlation has been reported between ADC and tumor differentiation.[72] DWI has also been reported as the most sensitive MRI sequence for the detection of liver metastases of neuroendocrine tumors.[73]

PANCREATIC CYSTIC LESIONS—DWI cannot be recommended for characterization of pancreatic cystic lesions, given the conflicting data.[66]

In summary, DWI improves the sensitivity of MRI of the pancreas for the detection of focal solid lesions. Quantitative diffusion parameters are promising for the differential diagnosis of focal parenchymal solid lesions. The role of DWI in assessing complications of pancreatitis should be further investigated.

Renal DWI

The kidney is a particularly interesting organ to assess by DWI because of its high blood flow and water transport functions.[74] DWI acquisition can be performed in the axial or coronal plane, using FB or RT acquisition.

CHARACTERIZATION OF RENAL LESIONS—A previous study compared the performance of CE-T_1WI and DWI when differentiating between benign cystic lesions, papillary and nonpapillary renal cell carcinomas (RCC) (Fig. 7), angiomyolipomas, and oncocytomas.[75] It was found that DWI (area under the curve [AUC]: 0.856; sensitivity: 86%; specificity: 80%) represents a reasonable, albeit less accurate, alternative to CE-MRI (AUC: 0.944; sensitivity: 100%; specificity: 89%) when characterizing renal masses. The diagnostic use of DWI is particularly relevant for patients with contraindications to gadolinium-based contrast agents (at risk for nephrogenic systemic fibrosis). However, DWI may generally provide additional information to radiologists: the same study showed that the combined use of DWI and CE-MRI led to an increased specificity of 96% compared to a specificity of 89% for CE-MRI alone. A retrospective study in 83 patients focused on the use of ADC measurements to differentiate between subtypes of RCC.[76] Interestingly, mean ADC values were computed for each lesion based on b values of 0 and 500 and of 0 and 800 s/mm^2. It was found that clear-cell RCC was associated with significantly higher ADC values compared with papillary and chromophobic RCC for both sets of b values ($P <$ 0.001). However, using b values of 0 and 800 sec/mm^2 was more effective for distinguishing

clear-cell RCC from nonclear-cell RCC (AUC: 0.973; sensitivity: 96%; specificity: 94%). It also led to significant differences in ADC values being found between papillary and chromophobic RCC ($P < 0.001$), while this was not the case for b values of 0 and 500 sec/mm^2. This study indicates that results may not be reproducible if different combinations of b values are used.

DIFFUSE RENAL DISEASES—Diffuse renal diseases can be detected by morphological analysis only at advanced stages, which often leads to a delay in adequate treatment. DWI has shown promising results for the evaluation of acute and chronic renal failure with decreased ADC values reported in this group of patients compared to healthy volunteers. A recent prospective study in 71 patients with chronic kidney disease determined that ADC values were negatively correlated with pathology scores and significantly different among three groups of patients with different degrees or renal impairment ($P < 0.001$).[77] The feasibility and reproducibility of DWI in transplanted kidneys have already been demonstrated[78] and initial results seem to be promising for the assessment of allograft deterioration.[79] A recent study in 137 healthy participants concluded that ADC values in the kidney may also be age- and gender-dependent.[80] These findings suggest the need for greater standardization in DWI and for large studies in which differences in ADC measurements are analyzed by age group and gender.

In summary, although morphological MRI and CT are excellent imaging modalities in the diagnostic work-up of a vast variety of renal pathologies, DWI shows promising results as a noninvasive and sensitive technique to provide information beyond morphology.

Prostate DWI

DWI substantially improves localization of dominant tumors in the prostate and has served as an essential factor in the greatly expanded role of MRI in clinical management of prostate cancer over the last decade. DWI exhibits high sensitivity for high-grade tumor, yet low sensitivity for low-grade tumor,[81] thereby helping to select patients with aggressive tumor for treatment while reducing overdiagnosis. ADC values obtained from DWI are inversely correlated with Gleason score[82] and are associated with tumor progression while on active surveillance[83] as well as with relapse following radiation or radical prostatectomy.[84]

Historically, prostate DWI was acquired using a maximal b-value of 700–1000 sec/mm^2. Unsuppressed signal of benign prostate tissue within this b-value range obscures increased signal in tumors. However, improvements in scanner and sequence technology have facilitated acquisition at even higher b-values of 1400–2000 sec/mm^2.[85] These "ultra"-high b-values achieve greater suppression of benign prostate tissue, providing improved tumor conspicuity and localization.[85] A particular role of ultra-high b-value images is to help differentiate benign prostatic hyperplasia from transition zone tumors.[85] In addition, the ultra-high b-value images can be synthesized from images obtained using standard b-values rather than directly acquired (Fig. 8). This process entails no additional acquisition time in comparison with that required for acquisition of the standard b-value images and is useful if encountering excessive artifact or insufficient SNR when directly acquiring ultra-high b-value images. However, it should be noted that synthesized high b-value images are only

extrapolations of low b-value behavior, which may provide contrast variation relative to surrounding tissue but no additional quantification or representation of true high b-value behavior (eg, kurtosis effects). Thus, their use should be applied carefully and qualitatively.

The MRI Prostate Imaging and Reporting Data System (PI-RADS) version 2 seeks to standardize prostate MRI interpretations.[86] In this system, the criteria for assigning a 1–5 suspicion score on DWI reflect a composite assessment of both the ADC map and ultra-high b-value images (whether acquired or synthesized). A peripheral zone lesion's score on DWI serves as the dominant score in determining its overall suspicion category. However, in the transition zone, T_2WI is the dominant sequence and determines the overall score in most instances.

Prostate DWI is prone to anatomic distortion and susceptibility-related artifact, given the EPI acquisition. Rectal gas is a key factor in exacerbating such issues, particularly during non-endorectal coil imaging. A number of interventions may help reduce this artifact, including the use of laxatives or enema, instruction to evacuate prior to imaging, and use of a suction catheter at the start of the examination to remove any rectal gas that remains despite these interventions.

Breast DWI

Technical considerations for breast DWI include optimizing acquisition protocols to achieve good image quality and appropriate b-value selection. EPI-based DWI sequences are susceptible to image distortion and ghosting artifacts, which are particularly problematic for breast imaging due to off-center imaging, air–tissue interfaces, and high fat content in the breast. To reduce artifacts and optimize data quality, good shimming and suppression of lipid signal are essential. Advanced RF coil design, parallel imaging, and higher-order shimming techniques help to overcome some of the unique challenges of breast DWI, particularly at higher field strengths. Currently, spatial distortion and lower resolution prevent direct correlation and one-to-one mapping of DCE-MRI and DWI features and limit clinical implementation of breast DWI, although a variety of new DWI acquisition strategies are under development to address these issues.

The choice of b values directly affects SNR and quantitative ADC analysis, and may vary according to the application. For lesion conspicuity and detection purposes, a high maximum b-value (800 s/mm^2) may be preferred,[87] while for differentiation between benign and malignant lesions, the choice of b-value may be less important.[87,88] DWI acquisition using multiple b values provides a more accurate sampling of signal decay for calculation of ADC, and use of a nonzero minimum b value reference image can help eliminate contaminations from perfusion and flow. However, studies investigating these approaches have not clearly demonstrated a clinical diagnostic advantage in breast imaging.[88] Given the time constraints of clinical practice, ADC calculation using two b-values (eg, b = 0, 800 s/mm^2) may be acceptable.

BREAST LESION DETECTION AND CHARACTERIZATION—Breast malignancies demonstrate restricted diffusion, with high signal intensity on DWI and low ADC values, attributed to increased cellularity and decreased extracellular space (Fig. 9). The most

widely explored application of DWI for breast imaging has been as an adjunct MRI technique to reduce false positives and unnecessary biopsies associated with DCE-MRI. Numerous groups have demonstrated significant differences in ADC values of benign and malignant lesions and shown that ADC measures can improve diagnostic accuracy of conventional DCE-MRI.[89] DWI may also offer a viable noncontrast method of breast MR screening without the costs and potential toxicity associated with DCE-MRI. Many mammographically and clinically occult breast cancers detected by DCE-MRI are also visible on DWI. In one study of asymptomatic women, DWI provided higher accuracy than screening mammography for the detection of breast malignancies.[90]

Treatment Monitoring

Cytotoxic effects of neoadjuvant chemotherapy cause significant alterations in cell membrane integrity and reduced tumor cellularity, resulting in an increase in water mobility within the damaged tumor tissue. Increases in breast tumor ADC in response to treatment are detectable earlier than changes in tumor size on MRI, suggesting that ADC may be a valuable early indicator of treatment efficacy.[91] While a number of studies have shown promising associations of breast tumor ADC measures with outcomes to therapy, reports in the literature have been varied and more work is needed to validate DWI as a useful biomarker of treatment response in breast cancer.

DWI in Gynecological Disease

DWI should be corroborated with standard imaging sequences for the assessment of gynecological malignancies. A sagittal acquisition plane is suggested for assessing endometrial and cervical cancer, while axial acquisition is suggested for evaluating adnexal/ovarian pathology and for lymph node detection.

MYOMETRIAL TUMOR CHARACTERIZATION—The differentiation between benign and malignant myometrial tumors on nonenhanced and postcontrast standard MRI sequences may be difficult, with an overall accuracy of ~69%. A recent study has demonstrated the added value of DWI to improve characterization.[92] In our experience, when a myometrial tumor displays a low T_2 signal and/or a low DW signal, the tumor is always benign. If the tumor displays high or intermediate T_2 signal and high DW signal, an ADC map helps differentiate benign from malignant tumors.[93]

ENDOMETRIAL CANCER (FIG. 10)—Staging of endometrial cancer requires assessment of the depth of myometrial invasion, which strongly correlates with lymph node metastases. It has been shown that a fused T_2 and axial oblique DWI perpendicular to the long axis of the myometrium is more accurate for assessment of myometrial invasion in comparison with T_2WI or DCE-MRI.[94] Moreover, DWI is helpful for detection of peritoneal implants.

CERVICAL CANCER—DWI is useful for detection of tumors not apparent on T_2WI, particularly in young patients with a diffusely infiltrating adenocarcinoma. In addition, DWI is a more sensitive technique than T_2WI for detection of small residual tumor after

chemoradiation therapy before surgery.[95] Finally, DWI is useful after the end of therapy, to differentiate tumor recurrence from fibrosis.[95]

OVARIAN PATHOLOGY—Several groups have investigated the ability of DWI for characterization of ovarian tumors. In our experience, both malignant and benign tumors may display high residual signal on high b value images (eg, b1000), while the absence of high b1000 signal is highly predictive of benignancy.[96] On the other hand, a tumor displaying both low T_2 and low DWI signal is generally benign. The addition of DWI to conventional sequences increases the diagnostic confidence in 15% of cases.[97] A second application of DWI has been in the assessment of peritoneal spread of gynecological malignancy with better contrast than on CT or conventional MRI. Finally, DWI may be useful to evaluate the early response to neoadjuvant chemotherapy in ovarian cancer with an increase in ADC after the first cycle of treatment.[98]

Spine DWI

The vertebral bone marrow is composed of three main elements: fatty marrow, hematopoietic marrow, and trabecular bone. The special tissue properties of the bone marrow and the complex anatomy of the spine result in differences in magnetic susceptibility, which complicates MRI, especially EPI techniques. However, with advances in EPI techniques, such as improved gradient systems, parallel imaging, and dynamic shimming, sagittal SS EPI has become a fairly robust tool.[99] Other DW pulse sequences such as segmented EPI techniques and SS FSE sequences are possible alternatives. A precise ADC measurement can still be difficult and large variations are found in the literature, mainly explained by acquisition parameter differences.[99]

DWI is a powerful addition to the arsenal of MRI techniques for the detection of bone marrow tumor dissemination, improving sensitivity for detecting bone metastases in a variety of tumor types[100] (Fig. 11). DWI increases confidence in monitoring treatment response and assisting in the differentiation of treatment-related changes from tumor, and therefore has become an important component of whole-body MRI oncology protocols (Fig. 12).

Distinguishing between benign and malignant etiologies of vertebral fractures with MRI is problematic, particularly if only one vertebra is affected. The value of DWI in discriminating between osteoporotic and metastatic vertebral fractures is controversial and insufficiently reliable.[101,102]

DWI is useful in differentiating degenerative and infectious endplate abnormalities. Symptomatic degenerative vertebral endplate signal changes (Modic type 1) can be difficult to differentiate from acute spondylodiscitis using conventional MRI techniques. Recently, a characteristic DWI finding of well-margined, linear, typically paired regions of high signal at the interface of normal with abnormal marrow, referred to as a "claw" sign, has been shown to be highly suggestive of degeneration and its absence in cases with Modic type I changes strongly suggestive of diskitis/osteomyelitis.[103]

Oncologic Treatment Response and Whole-Body DWI

The assessment of tumor response to oncologic treatment is still largely based on size measurement criteria or modification of these.[104] However, with the growing use of cytostatic treatments, tumor size measurements are becoming insensitive to efficacy effects and there is a need for new imaging biomarkers to assess treatment effectiveness. DWI can determine the success of treatments through alterations in tumor size/volume, signal intensity, and ADC changes. Numerous studies have shown that ADC values in a number of tumor types (including brain, lung, liver metastases, HCC, pancreas, kidneys, cervix, uterine, prostate, lymphoma, sarcoma, and primary and secondary bone malignancies) increases with effective treatments, which include chemotherapy, radiotherapy, novel targeted treatments, embolization, and radiofrequency ablation. ADC increase often precede reductions in tumor size, and may be observed as early as 1–4 weeks of initiating treatment.[105] However, the magnitude and temporal evolution of ADC change depends on the mechanism of action of the treatment, with those resulting in profound cell kill resulting in the most rapid and largest increases in the ADC values.

A major strength of ADC measurements in the body is its measurement repeatability. In well-conducted studies, using free-breathing techniques, the test–retest repeatability of ADC measurements in single-center and cross-center studies have been shown to be good. Bland–Altman analyses show that the coefficient of repeatability is typically about 15–30% across multiple studies. More recently, the relatively robust nature of ADC measurements was shown within and between vendors, for machines operating at both 1.5T and 3.0T.[106] The intervendor repeatability was also shown in one study to be about 14%.[106] However, the measurement repeatability of quantitative DWI indices derived using more complex diffusion models (eg, IVIM and DKI) can be poor, and it is important to apply complex models judiciously, considering aspects of image SNR, disease type, and treatment contexts.

A key unmet clinical need is for a robust biomarker to assess the treatment effectiveness of bone metastases, especially for prostate and breast cancers.[107] This is because radionuclide bone scans do not directly identify metastases (bone scan uptake is a marker of osteoblastic activity) and there are no accepted bone scan criteria for defining therapy benefit. As a result, patients are treated to documented progression (defined clinically and with imaging), often resulting in unrecognized tumor burdens and delays before treatment changes are instituted. This need can potentially be met by whole-body MRI methods. Whole-body DWI is technically feasible across vendor systems and can be undertaken at both 1.5T and 3.0T (Fig. 12). Visual assessments of the inverted gray scale maximum intensity projection images can be used to appraise treatment effects, with treatment response showing reductions in high b-value signal intensity (Fig. 13). In addition, the DWI signal intensity of bone metastases can be used for disease volume segmentation and global ADC quantification.[108] Effective treatments are associated with reductions in disease volume accompanying rises in the ADC values. Importantly, whole-body imaging enables heterogeneity of response to be documented (commonly seen in the metastatic setting after several lines of treatments). However, the criteria for defining bone metastasis response, stable disease, and disease progression using DWI are being established. It is likely that this would require a combination of imaging criteria, which may include changes in bone

marrow fat fraction, signal intensity changes on conventional T_1 and T_2WI, as well as DWI signal and ADC measurement characteristics.[107]

Future Directions

IVIM DWI: Potential Body Imaging Applications

There is considerable recent literature on the use of IVIM, which employs a biexponential diffusion model to estimate capillary contributions to the DW signal.[40,42,109] IVIM has the potential to help characterize diffuse liver disease,[37,38] focal liver and pancreatic lesions,[110,111] and renal function[112] (Fig. 2). IVIM is increasingly applied in a wide variety of cancer types, due to their typically hypervascular and hypercellular features.[32,110,113] Data showing superiority of IVIM parameters over ADC for tissue characterization is limited, and more evidence is needed. IVIM parameter reproducibility and the role of IVIM parameters in treatment response need also to be better defined. In addition, the biological significance of IVIM-related "perfusion" needs to be better understood.

Diffusion Kurtosis Imaging (DKI)

While diffusion data are most commonly processed using a standard monoexponential fit to obtain the parameter ADC, this model may not in fact optimally fit the raw diffusion data. Other more sophisticated models have been investigated, including the biexponential and stretched exponential diffusion models, in efforts to obtain more reliable estimates of tissue diffusivity. However, these models do not reflect the non-Gaussian (non-"free") behavior of water diffusion that manifests at ultra-high b-values and is believed to provide additional insights into tissue architecture.[114] Recent publications employing higher b-values have shown advantages in using DKI, a model of diffusion that characterizes the excess kurtosis from non-Gaussian diffusion propagators in breast, prostate, and pancreatic studies.[115,116] While largely applied for brain imaging, DKI has more recently been investigated in body imaging. The primary such application has been in the prostate, in which greater performance for differentiating low- and high-grade prostate cancer using K than standard ADC obtained from a monoexponential fit has been observed.[117] DKI has also been preliminarily explored for tumor characterization in the breast as well as the head and neck. While hardware improvements have allowed for better quality of DWI performed at very high b-values of ~2000 s/mm^2 and thereby facilitated the clinical application of DKI in recent years, great attention to acquisition detail is important to ensure sufficient SNR at the maximal b-values, and thus reliability of the computed metrics. In addition, the exact microstructural property of tissue represented by K_{app}, like the ADC, depends on the tissue architecture studied; higher specificity is therefore expected when DKI is combined with a biophysical model.

DWI and PET/MRI

PET/MRI is a novel hybrid imaging modality, combining the morphological, functional, and molecular imaging potential of MRI and PET. The combination with DWI is an excellent example for the true potential of PET/MR, as it allows for insights into tissue structure and biology, which are not possible with PET/CT.[118] There are generally two different strategies of combining DWI and PET in PET/MR. One can use the excellent sensitivity of DWI for

lesion detection and combine it with PET. However, for whole-body imaging, adding DWI to a PET/MR protocol might be quite time-consuming, unless a very brief DWI protocol is employed. This only makes sense when one expects truly synergistic information. It has been suggested that combining two excellent staging modalities may not always provide complementary but rather redundant information.

A classic example would be primary staging in an FDG-avid malignancy where usually FDG is sufficient for tumor detection and DWI adds little information.[119] However, the situation is different when PET is used to gather biological information with specific tracers, like FLT (fluorothymidine)-PET for assessment of tumor proliferation or receptor imaging. In these cases lesions might be negative in PET but could still be picked up with whole-body DWI, thus synergistically combining lesion detection and characterization. More practical and less time-consuming for PET/MR in oncology is region-specific DWI. This means that DWI is only added to the MR protocol for a specific area of interest, where PET might be limited for lesion detection, like in the liver, to rule out small liver metastases. However, the true potential of combining DWI and PET in PET/MR lies not so much in lesion detection, as described above, but to make maximum use of the quantitative information on tissue biology one gets in a single examination with optimum image coregistration. By analyzing the data on restricted water movement and tracer uptake on a voxel-by-voxel basis, a novel set of biomarkers might evolve, which add synergistic information on tumor biology to the classical biomarkers derived from tissue biopsy or liquid biopsy.[120] Compared to the latter, PET/MR-derived biomarkers have several advantages, like being minimally invasive, allowing for serial whole-body assessment, and depicting intra- and interlesional heterogeneity. This method could be helpful for biopsy guidance, prognostic assessment, radiation therapy planning, or response evaluation (Fig. 14).

Conclusion

The 2015 ISMRM-sponsored workshop has stimulated in-depth discussions of body DWI and the current state of the art. The key points are summarized below:

- Body DWI is no longer direct transportation of methods from the brain but an adaptation to specific challenges and opportunities of extracranial anatomies and pathologies.

- Validated quality control metrics are available to quantify measurement repeatability, reproducibility, and precision of quantitative DWI. ADC measurements outside the brain show good to excellent measurement repeatability, although more data on interplatform reproducibility are needed.

- Perfusion insensitive ADC (eg, obtained from b-values between 50 and 1000 s/mm^2) is robust and can be recommended for general evaluation.

- DWI has been shown to improve disease assessment in the liver, pancreas, kidneys, prostate, breast, gynecological diseases, and spine.

- • DWI (including whole-body DWI) shows substantial promise for assessing tumor response in oncology, although larger prospective studies are needed to qualify ADC as a response biomarker.

- • Under appropriate measurement conditions, non-monoexponential diffusion models (eg, IVIM, DKI, and stretched exponential) could be explored to provide further tissue characterization, particularly in oncological applications.

- • Further exploration of non-monoexponential diffusion models and combination with PET imaging would further enhance the value of DWI in the body.

References

1. Padhani AR, Liu G, Koh DM, et al. Diffusion-weighted magnetic resonance imaging as a cancer biomarker: consensus and recommendations. Neoplasia. 2009; 11:102–125. [PubMed: 19186405]

2. Haacke, EM.; Brown, RW.; Thompson, MR.; Venkatesan, R. Magnetic resonance imaging: physical principles and sequence design. New York: John Wiley & Sons; 1999.

3. Zech CJ, Herrmann KA, Dietrich O, Horger W, Reiser MF, Schoenberg SO. Black-blood diffusion-weighted EPI acquisition of the liver with parallel imaging — comparison with a standard T2-weighted sequence for detection of focal liver lesions. Invest Radiol. 2008; 43:261–266. [PubMed: 18340250]

4. Fillmer A, Kirchner T, Cameron D, Henning A. Constrained image-based B0 shimming accounting for "local minimum traps" in the optimization and field inhomogeneities outside the region of interest. Magn Reson Med. 2015; 73:1370–1380. [PubMed: 24715495]

5. Lu Y, Hatzoglou V, Banerjee S, et al. Repeatability investigation of reduced field-of-view diffusion-weighted magnetic resonance imaging on thyroid glands. J Comput Assist Tomogr. 2015; 39:334–339. [PubMed: 25700226]

6. Ma C, Li YJ, Pan CS, et al. High resolution diffusion weighted magnetic resonance imaging of the pancreas using reduced field of view single-shot echo-planar imaging at 3T. Magn Reson Imaging. 2014; 32:125–131. [PubMed: 24231348]

7. Jin N, Deng J, Zhang LJ, et al. Targeted single-shot methods for diffusion-weighted imaging in the kidneys. J Magn Reson Imaging. 2011; 33:1517–1525. [PubMed: 21591023]

8. Singer L, Wilmes LJ, Saritas EU, et al. High-resolution diffusion-weighted magnetic resonance imaging in patients with locally advanced breast cancer. Acad Radiol. 2012; 19:526–534. [PubMed: 22197382]

9. Wilmes LJ, McLaughlin RL, Newitt DC, et al. High-resolution diffusion-weighted imaging for monitoring breast cancer treatment response. Acad Radiol. 2013; 20:581–589. [PubMed: 23570936]

10. Wilm BJ, Gamper U, Henning A, Pruessmann KP, Kollias SS, Boesiger P. Diffusion-weighted imaging of the entire spinal cord. NMR Biomed. 2009; 22:174–181. [PubMed: 18727164]

11. Rao RK, Riffel P, Meyer M, et al. Implementation of dual-source RF excitation in 3 T MR-scanners allows for nearly identical ADC values compared to 1.5 T MR scanners in the abdomen. PLoS One. 2012; 7:e32613. [PubMed: 22393422]

12. Holdsworth SJ, Skare S, Newbould RD, Bammer R. Robust GRAPPA-accelerated diffusion-weighted readout-segmented (RS)-EPI. Magn Reson Med. 2009; 62:1629–1640. [PubMed: 19859974]

13. Deng J, Miller FH, Salem R, Omary RA, Larson AC. Multishot diffusion-weighted PROPELLER magnetic resonance imaging of the abdomen. Invest Radiol. 2006; 41:769–775. [PubMed: 16971801]

14. Deng J, Omary RA, Larson AC. Multishot diffusion-weighted SPLICE PROPELLER MRI of the abdomen. Magn Reson Med. 2008; 59:947–953. [PubMed: 18429036]

15. Liu C, Bammer R, Kim DH, Moseley ME. Self-navigated interleaved spiral (SNAILS): application to high-resolution diffusion tensor imaging. Magn Reson Med. 2004; 52:1388–1396. [PubMed: 15562493]

16. Porter DA, Heidemann RM. High resolution diffusion-weighted imaging using readout-segmented echo-planar imaging, parallel imaging and a two-dimensional navigator-based reacquisition. Magn Reson Med. 2009; 62:468–475. [PubMed: 19449372]

17. Tokoro H, Fujinaga Y, Ohya A, et al. Usefulness of free-breathing readout-segmented echo-planar imaging (RESOLVE) for detection of malignant liver tumors: comparison with single-shot echo-planar imaging (SS-EPI). Eur J Radiol. 2014; 83:1728–1733. [PubMed: 25043495]

18. Wisner DJ, Rogers N, Deshpande VS, et al. High-resolution diffusion-weighted imaging for the separation of benign from malignant BI-RADS 4/5 lesions found on breast MRI at 3T. J Magn Reson Imaging. 2014; 40:674–681. [PubMed: 24214467]

19. Jeong EK, Kim SE, Kholmovski EG, Parker DL. High-resolution DTI of a localized volume using 3D single-shot diffusion-weighted stimulated echo-planar imaging (3D ss-DWSTEPI). Magn Reson Med. 2006; 56:1173–1181. [PubMed: 17089367]

20. Karampinos DC, Banerjee S, King KF, Link TM, Majumdar S. Considerations in high-resolution skeletal muscle diffusion tensor imaging using single-shot echo planar imaging with stimulated-echo preparation and sensitivity encoding. NMR Biomed. 2012; 25:766–778. [PubMed: 22081519]

21. Sigmund EE, Sui D, Ukpebor O, et al. Stimulated echo diffusion tensor imaging and SPAIR T2-weighted imaging in chronic exertional compartment syndrome of the lower leg muscles. J Magn Reson Imaging. 2013; 38:1073–1082. [PubMed: 23440764]

22. Sigmund EE, Novikov DS, Sui D, et al. Time-dependent diffusion in skeletal muscle with the random permeable barrier model (RPBM): application to normal controls and chronic exertional compartment syndrome patients. NMR Biomed. 2014; 27:519–528. [PubMed: 24610770]

23. Novikov DS, Fieremans E, Jensen JH, Helpern JA. Random walks with barriers. Nat Phys. 2011; 7:508–514. [PubMed: 21686083]

24. Chenevert TL, Galban CJ, Ivancevic MK, et al. Diffusion coefficient measurement using a temperature-controlled fluid for quality control in multicenter studies. J Magn Reson Imaging. 2011; 34:983–987. [PubMed: 21928310]

25. Kivrak AS, Paksoy Y, Erol C, Koplay M, Ozbek S, Kara F. Comparison of apparent diffusion coefficient values among different MRI platforms: a multicenter phantom study. Diagn Interv Radiol. 2013; 19:433–437. [PubMed: 24004973]

26. Malyarenko D, Galban CJ, Londy FJ, et al. Multi-system repeatability and reproducibility of apparent diffusion coefficient measurement using an ice-water phantom. J Magn Reson Imaging. 2013; 37:1238–1246. [PubMed: 23023785]

27. Malyarenko DI, Newitt D, L JW, et al. Demonstration of nonlinearity bias in the measurement of the apparent diffusion coefficient in multicenter trials. Magn Reson Med. 2015 [Epub ahead of print].

28. Sasaki M, Yamada K, Watanabe Y, et al. Variability in absolute apparent diffusion coefficient values across different platforms may be substantial: a multivendor, multi-institutional comparison study. Radiology. 2008; 249:624–630. [PubMed: 18936317]

29. Braithwaite AC, Dale BM, Boll DT, Merkle EM. Short- and midterm reproducibility of apparent diffusion coefficient measurements at 3.0-T diffusion-weighted imaging of the abdomen. Radiology. 2009; 250:459–465. [PubMed: 19095786]

30. Corona-Villalobos CP, Pan L, Halappa VG, et al. Agreement and reproducibility of apparent diffusion coefficient measurements of dual-b-value and multi-b-value diffusion-weighted magnetic resonance imaging at 1.5 Tesla in phantom and in soft tissues of the abdomen. J Comput Assist Tomogr. 2013; 37:46–51. [PubMed: 23321832]

31. Koh DM, Blackledge M, Collins DJ, et al. Reproducibility and changes in the apparent diffusion coefficients of solid tumours treated with combretastatin A4 phosphate and bevacizumab in a two-centre phase I clinical trial. Eur Radiol. 2009; 19:2728–2738. [PubMed: 19547986]

32. Kakite S, Dyvorne H, Besa C, et al. Hepatocellular carcinoma: Short-term reproducibility of apparent diffusion coefficient and intravoxel incoherent motion parameters at 3.0T. J Magn Reson Imaging. 2015; 41:149–156. [PubMed: 24415565]

33. Le Bihan D, Breton E, Lallemand D, Grenier P, Cabanis E, Laval-Jeantet M. MR imaging of intravoxel incoherent motions: application to diffusion and perfusion in neurologic disorders. Radiology. 1986; 161:401–407. [PubMed: 3763909]

34. Koh DM, Collins DJ, Orton MR. Intravoxel incoherent motion in body diffusion-weighted MRI: reality and challenges. AJR Am J Roentgenol. 2011; 196:1351–1361. [PubMed: 21606299]

35. Le Bihan D, Breton E, Lallemand D, Aubin ML, Vignaud J, Laval-Jeantet M. Separation of diffusion and perfusion in intravoxel incoherent motion MR imaging. Radiology. 1988; 168:497–505. [PubMed: 3393671]

36. Iima M, Le Bihan D. Clinical intravoxel incoherent motion and diffusion MR imaging: past, present, and future. Radiology. 2016; 278:13–32. [PubMed: 26690990]

37. Luciani A, Vignaud A, Cavet M, et al. Liver cirrhosis: intravoxel incoherent motion MR imaging—pilot study. Radiology. 2008; 249:891–899. [PubMed: 19011186]

38. Patel J, Sigmund EE, Rusinek H, Oei M, Babb JS, Taouli B. Diagnosis of cirrhosis with intravoxel incoherent motion diffusion MRI and dynamic contrast-enhanced MRI alone and in combination: preliminary experience. J Magn Reson Imaging. 2010; 31:589–600. [PubMed: 20187201]

39. Lemke A, Stieltjes B, Schad LR, Laun FB. Toward an optimal distribution of b values for intravoxel incoherent motion imaging. Magn Reson Imaging. 2011; 29:766–776. [PubMed: 21549538]

40. Cho GY, Moy L, Zhang JL, et al. Comparison of fitting methods and b-value sampling strategies for intravoxel incoherent motion in breast cancer. Magn Reson Med. 2015; 74:1077–1085. [PubMed: 25302780]

41. Dyvorne HA, Galea N, Nevers T, et al. Diffusion-weighted imaging of the liver with multiple b values: effect of diffusion gradient polarity and breathing acquisition on image quality and intravoxel incoherent motion parameters—a pilot study. Radiology. 2013; 266:920–929. [PubMed: 23220895]

42. Dyvorne H, Jajamovich G, Kakite S, Kuehn B, Taouli B. Intravoxel incoherent motion diffusion imaging of the liver: optimal b-value sub-sampling and impact on parameter precision and reproducibility. Eur J Radiol. 2014; 83:2109–2113. [PubMed: 25277521]

43. Zhang JL, Sigmund EE, Rusinek H, et al. Optimization of b-value sampling for diffusion-weighted imaging of the kidney. Magn Reson Med. 2012; 67:89–97. [PubMed: 21702062]

44. Merisaari H, Jambor I. Optimization of b-value distribution for four mathematical models of prostate cancer diffusion-weighted imaging using b values up to 2000 s/mm(2): simulation and repeatability study. Magn Reson Med. 2015; 73:1954–1969. [PubMed: 25045885]

45. Notohamiprodjo M, Glaser C, Herrmann KA, et al. Diffusion tensor imaging of the kidney with parallel imaging: initial clinical experience. Invest Radiol. 2008; 43:677–685. [PubMed: 18791409]

46. Andreou A, Koh DM, Collins DJ, et al. Measurement reproducibility of perfusion fraction and pseudodiffusion coefficient derived by intravoxel incoherent motion diffusion-weighted MR imaging in normal liver and metastases. Eur Radiol. 2013; 23:428–434. [PubMed: 23052642]

47. Jerome NP, Orton MR, d'Arcy JA, Collins DJ, Koh DM, Leach MO. Comparison of free-breathing with navigator-controlled acquisition regimes in abdominal diffusion-weighted magnetic resonance images: effect on ADC and IVIM statistics. J Magn Reson Imaging. 2014; 39:235–240. [PubMed: 23580454]

48. Lee Y, Lee SS, Kim N, et al. Intravoxel incoherent motion diffusion-weighted MR imaging of the liver: effect of triggering methods on regional variability and measurement repeatability of quantitative parameters. Radiology. 2015; 274:405–415. [PubMed: 25232802]

49. Kiselev VG, Il'yasov KA. Is the "biexponential diffusion" biexponential? Magn Reson Med. 2007; 57:464–469. [PubMed: 17326171]

50. Jensen JH, Helpern JA. MRI quantification of non-Gaussian water diffusion by kurtosis analysis. NMR Biomed. 2010; 23:698–710. [PubMed: 20632416]

51. Rosenkrantz AB, Padhani AR, Chenevert TL, et al. Body diffusion kurtosis imaging: Basic principles, applications, and considerations for clinical practice. J Magn Reson Imaging. 2015; 42:1190–1202. [PubMed: 26119267]

52. Bennett KM, Schmainda KM, Bennett RT, Rowe DB, Lu H, Hyde JS. Characterization of continuously distributed cortical water diffusion rates with a stretched-exponential model. Magn Reson Med. 2003; 50:727–734. [PubMed: 14523958]

53. Winfield JM, deSouza NM, Priest AN, et al. Modelling DW-MRI data from primary and metastatic ovarian tumours. Eur Radiol. 2015; 25:2033–2040. [PubMed: 25605133]

54. Kwee TC, Galban CJ, Tsien C, et al. Comparison of apparent diffusion coefficients and distributed diffusion coefficients in high-grade gliomas. J Magn Reson Imaging. 2010; 31:531–537. [PubMed: 20187193]

55. Bennett KM, Hyde JS, Schmainda KM. Water diffusion heterogeneity index in the human brain is insensitive to the orientation of applied magnetic field gradients. Magn Reson Med. 2006; 56:235–239. [PubMed: 16929466]

56. Yablonskiy DA, Bretthorst GL, Ackerman JJ. Statistical model for diffusion attenuated MR signal. Magn Reson Med. 2003; 50:664–669. [PubMed: 14523949]

57. Choi JS, Kim MJ, Choi JY, Park MS, Lim JS, Kim KW. Diffusion-weighted MR imaging of liver on 3.0-Tesla system: effect of intravenous administration of gadoxetic acid disodium. Eur Radiol. 2010; 20:1052–1060. [PubMed: 19915849]

58. Chiu FY, Jao JC, Chen CY, et al. Effect of intravenous gadolinium-DTPA on diffusion-weighted magnetic resonance images for evaluation of focal hepatic lesions. J Comput Assist Tomogr. 2005; 29:176–180. [PubMed: 15772533]

59. Taouli B, Koh DM. Diffusion-weighted MR imaging of the liver. Radiology. 2010; 254:47–66. [PubMed: 20032142]

60. Taouli B, Vilgrain V, Dumont E, Daire JL, Fan B, Menu Y. Evaluation of liver diffusion isotropy and characterization of focal hepatic lesions with two single-shot echo-planar MR imaging sequences: prospective study in 66 patients. Radiology. 2003; 226:71–78. [PubMed: 12511671]

61. Parikh T, Drew SJ, Lee VS, et al. Focal liver lesion detection and characterization with diffusion-weighted MR imaging: comparison with standard breath-hold T2-weighted imaging. Radiology. 2008; 246:812–822. [PubMed: 18223123]

62. Wu LM, Hu J, Gu HY, Hua J, Xu JR. Can diffusion-weighted magnetic resonance imaging (DW-MRI) alone be used as a reliable sequence for the preoperative detection and characterisation of hepatic metastases? A meta-analysis. Eur J Cancer. 2013; 49:572–584. [PubMed: 23000072]

63. Lewin M, Poujol-Robert A, Boelle PY, et al. Diffusion-weighted magnetic resonance imaging for the assessment of fibrosis in chronic hepatitis C. Hepatology. 2007; 46:658–665. [PubMed: 17663420]

64. Wang Y, Ganger DR, Levitsky J, et al. Assessment of chronic hepatitis and fibrosis: comparison of MR elastography and diffusion-weighted imaging. AJR Am J Roentgenol. 2011; 196:553–561. [PubMed: 21343496]

65. Dyvorne HA, Jajamovich GH, Bane O, et al. Prospective comparison of magnetic resonance imaging to transient elastography and serum markers for liver fibrosis detection. Liver Int. 2016 [Epub ahead of print].

66. Barral M, Taouli B, Guiu B, et al. Diffusion-weighted MR imaging of the pancreas: current status and recommendations. Radiology. 2015; 274:45–63. [PubMed: 25531479]

67. Shinya S, Sasaki T, Nakagawa Y, Guiquing Z, Yamamoto F, Yamashita Y. The efficacy of diffusion-weighted imaging for the detection and evaluation of acute pancreatitis. Hepatogastroenterology. 2009; 56:1407–1410. [PubMed: 19950800]

68. Islim F, Salik AE, Bayramoglu S, Guven K, Alis H, Turhan AN. Non-invasive detection of infection in acute pancreatic and acute necrotic collections with diffusion-weighted magnetic resonance imaging: preliminary findings. Abdom Imaging. 2014; 39:472–481. [PubMed: 24441591]

69. Park MJ, Kim YK, Choi SY, Rhim H, Lee WJ, Choi D. Preoperative detection of small pancreatic carcinoma: value of adding diffusion-weighted imaging to conventional MR imaging for improving confidence level. Radiology. 2014; 273:433–443. [PubMed: 24991989]

70. Kang KM, Lee JM, Yoon JH, Kiefer B, Han JK, Choi BI. Intravoxel incoherent motion diffusion-weighted MR imaging for characterization of focal pancreatic lesions. Radiology. 2014; 270:444–453. [PubMed: 24126370]

71. Schmid-Tannwald C, Schmid-Tannwald CM, Morelli JN, et al. Comparison of abdominal MRI with diffusion-weighted imaging to 68Ga-DOTATATE PET/CT in detection of neuroendocrine tumors of the pancreas. Eur J Nucl Med Mol Imaging. 2013; 40:897–907. [PubMed: 23460395]

72. Wang Y, Chen ZE, Yaghmai V, et al. Diffusion-weighted MR imaging in pancreatic endocrine tumors correlated with histopathologic characteristics. J Magn Reson Imaging. 2011; 33:1071–1079. [PubMed: 21509863]

73. d'Assignies G, Fina P, Bruno O, et al. High sensitivity of diffusion-weighted MR imaging for the detection of liver metastases from neuroendocrine tumors: comparison with T2-weighted and dynamic gadolinium-enhanced MR imaging. Radiology. 2013; 268:390–399. [PubMed: 23533288]

74. Thoeny HC, De Keyzer F. Diffusion-weighted MR imaging of native and transplanted kidneys. Radiology. 2011; 259:25–38. [PubMed: 21436095]

75. Taouli B, Thakur RK, Mannelli L, et al. Renal lesions: characterization with diffusion-weighted imaging versus contrast-enhanced MR imaging. Radiology. 2009; 251:398–407. [PubMed: 19276322]

76. Wang H, Cheng L, Zhang X, et al. Renal cell carcinoma: diffusion-weighted MR imaging for subtype differentiation at 3.0 T. Radiology. 2010; 257:135–143. [PubMed: 20713607]

77. Li Q, Li J, Zhang L, Chen Y, Zhang M, Yan F. Diffusion-weighted imaging in assessing renal pathology of chronic kidney disease: a preliminary clinical study. Eur J Radiol. 2014; 83:756–762. [PubMed: 24581595]

78. Thoeny HC, Zumstein D, Simon-Zoula S, et al. Functional evaluation of transplanted kidneys with diffusion-weighted and BOLD MR imaging: initial experience. Radiology. 2006; 241:812–821. [PubMed: 17114628]

79. Eisenberger U, Binser T, Thoeny HC, Boesch C, Frey FJ, Vermathen P. Living renal allograft transplantation: diffusion-weighted MR imaging in longitudinal follow-up of the donated and the remaining kidney. Radiology. 2014; 270:800–808. [PubMed: 24475796]

80. Suo ST, Cao MQ, Ding YZ, Yao QY, Wu GY, Xu JR. Apparent diffusion coefficient measurements of bilateral kidneys at 3 T MRI: effects of age, gender, and laterality in healthy adults. Clin Radiol. 2014; 69:e491–e496. [PubMed: 25239787]

81. Langer DL, van der Kwast TH, Evans AJ, et al. Intermixed normal tissue within prostate cancer: effect on MR imaging measurements of apparent diffusion coefficient and T2—sparse versus dense cancers. Radiology. 2008; 249:900–908. [PubMed: 19011187]

82. Gibbs P, Liney GP, Pickles MD, Zelhof B, Rodrigues G, Turnbull LW. Correlation of ADC and T2 measurements with cell density in prostate cancer at 3.0 Tesla. Invest Radiol. 2009; 44:572–576. [PubMed: 19692841]

83. van As NJ, de Souza NM, Riches SF, et al. A study of diffusion-weighted magnetic resonance imaging in men with untreated localised prostate cancer on active surveillance. Eur Urol. 2009; 56:981–987. [PubMed: 19095345]

84. Park JJ, Kim CK, Park SY, Park BK, Lee HM, Cho SW. Prostate cancer: role of pretreatment multiparametric 3-T MRI in predicting biochemical recurrence after radical prostatectomy. AJR Am J Roentgenol. 2014; 202:W459–W465. [PubMed: 24758681]

85. Katahira K, Takahara T, Kwee TC, et al. Ultra-high-b-value diffusion-weighted MR imaging for the detection of prostate cancer: evaluation in 201 cases with histopathological correlation. Eur Radiol. 2011; 21:188–196. [PubMed: 20640899]

86. American College of Radiology. Magnetic Resonance Prostate Imaging Reporting and Data System (MR PI-RADS). [Accessed on: May 21, 2015] http://www.acr.org/Quality-Safety/Resources/PIRADS.

87. Bogner W, Gruber S, Pinker K, et al. Diffusion-weighted MR for differentiation of breast lesions at 3.0T: how does selection of diffusion protocols affect diagnosis? Radiology. 2009; 253:341–351. [PubMed: 19703869]

88. Peters NH, Vincken KL, van den Bosch MA, Luijten PR, Mali WP, Bartels LW. Quantitative diffusion weighted imaging for differentiation of benign and malignant breast lesions: the influence of the choice of b-values. J Magn Reson Imaging. 2010; 31:1100–1105. [PubMed: 20432344]

89. Partridge SC, DeMartini WB, Kurland BF, Eby PR, White SW, Lehman CD. Quantitative diffusion-weighted imaging as an adjunct to conventional breast MRI for improved positive predictive value. AJR Am J Roentgenol. 2009; 193:1716–1722. [PubMed: 19933670]

90. Yabuuchi H, Matsuo Y, Sunami S, et al. Detection of non-palpable breast cancer in asymptomatic women by using unenhanced diffusion-weighted and T2-weighted MR imaging: comparison with mammography and dynamic contrast-enhanced MR imaging. Eur Radiol. 2011; 21:11–17. [PubMed: 20640898]

91. Sharma U, Danishad KK, Seenu V, Jagannathan NR. Longitudinal study of the assessment by MRI and diffusion-weighted imaging of tumor response in patients with locally advanced breast cancer undergoing neoadjuvant chemotherapy. NMR Biomed. 2009; 22:104–113. [PubMed: 18384182]

92. Tamai K, Koyama T, Saga T, et al. The utility of diffusion-weighted MR imaging for differentiating uterine sarcomas from benign leiomyomas. Eur Radiol. 2008; 18:723–730. [PubMed: 17929022]

93. Thomassin-Naggara I, Dechoux S, Bonneau C, et al. How to differentiate benign from malignant myometrial tumours using MR imaging. Eur Radiol. 2013; 23:2306–2314. [PubMed: 23563602]

94. Beddy P, Moyle P, Kataoka M, et al. Evaluation of depth of myometrial invasion and overall staging in endometrial cancer: comparison of diffusion-weighted and dynamic contrast-enhanced MR imaging. Radiology. 2012; 262:530–537. [PubMed: 22114239]

95. Nishie A, Stolpen AH, Obuchi M, Kuehn DM, Dagit A, Andresen K. Evaluation of locally recurrent pelvic malignancy: performance of T2- and diffusion-weighted MRI with image fusion. J Magn Reson Imaging. 2008; 28:705–713. [PubMed: 18777555]

96. Thomassin-Naggara I, Darai E, Cuenod CA, et al. Contribution of diffusion-weighted MR imaging for predicting benignity of complex adnexal masses. Eur Radiol. 2009; 19:1544–1552. [PubMed: 19214523]

97. Thomassin-Naggara I, Toussaint I, Perrot N, et al. Characterization of complex adnexal masses: value of adding perfusion- and diffusion-weighted MR imaging to conventional MR imaging. Radiology. 2011; 258:793–803. [PubMed: 21193596]

98. Kyriazi S, Collins DJ, Messiou C, et al. Metastatic ovarian and primary peritoneal cancer: assessing chemotherapy response with diffusion-weighted MR imaging—value of histogram analysis of apparent diffusion coefficients. Radiology. 2011; 261:182–192. [PubMed: 21828186]

99. Dietrich O, Geith T, Reiser MF, Baur-Melnyk A. Diffusion imaging of the vertebral bone marrow. NMR Biomed. 2015 [Epub ahead of print].

100. Nakanishi K, Kobayashi M, Nakaguchi K, et al. Whole-body MRI for Detecting Metastatic Bone Tumor: Diagnostic Value of Diffusion-weighted Images. Magn Reson Med Sci. 2007; 6:147–155. [PubMed: 18037795]

101. Castillo M, Arbelaez A, Smith JK, Fisher LL. Diffusion-weighted MR imaging offers no advantage over routine noncontrast MR imaging in the detection of vertebral metastases. AJNR Am J Neuroradiol. 2000; 21:948–953. [PubMed: 10815675]

102. Zhou XJ, Leeds NE, McKinnon GC, Kumar AJ. Characterization of benign and metastatic vertebral compression fractures with quantitative diffusion MR imaging. AJNR Am J Neuroradiol. 2002; 23:165–170. [PubMed: 11827890]

103. Patel KB, Poplawski MM, Pawha PS, Naidich TP, Tanenbaum LN. Diffusion-weighted MRI "claw sign" improves differentiation of infectious from degenerative modic type 1 signal changes of the spine. AJNR Am J Neuroradiol. 2014; 35:1647–1652. [PubMed: 24742801]

104. Eisenhauer EA, Therasse P, Bogaerts J, et al. New response evaluation criteria in solid tumours: revised RECIST guideline (version 1.1). Eur J Cancer. 2009; 45:228–247. [PubMed: 19097774]

105. Afaq A, Andreou A, Koh DM. Diffusion-weighted magnetic resonance imaging for tumour response assessment: why, when and how? Cancer Imaging. 2010; 10(Spec no A):S179–S188. [PubMed: 20880779]

106. Donati OF, Chong D, Nanz D, et al. Diffusion-weighted MR imaging of upper abdominal organs: field strength and intervendor variability of apparent diffusion coefficients. Radiology. 2014; 270:454–463. [PubMed: 24471390]

107. Padhani AR, Makris A, Gall P, Collins DJ, Tunariu N, de Bono JS. Therapy monitoring of skeletal metastases with whole-body diffusion MRI. J Magn Reson Imaging. 2014; 39:1049–1078. [PubMed: 24510426]

108. Blackledge MD, Collins DJ, Tunariu N, et al. Assessment of treatment response by total tumor volume and global apparent diffusion coefficient using diffusion-weighted MRI in patients with metastatic bone disease: a feasibility study. PLoS One. 2014; 9:e91779. [PubMed: 24710083]

109. Wurnig MC, Donati OF, Ulbrich E, et al. Systematic analysis of the intravoxel incoherent motion threshold separating perfusion and diffusion effects: proposal of a standardized algorithm. Magn Reson Med. 2015; 74:1414–1422. [PubMed: 25360990]

110. Lemke A, Laun FB, Klauss M, et al. Differentiation of pancreas carcinoma from healthy pancreatic tissue using multiple b-values: comparison of apparent diffusion coefficient and intravoxel incoherent motion derived parameters. Invest Radiol. 2009; 44:769–775. [PubMed: 19838121]

111. Yoon JH, Lee JM, Yu MH, Kiefer B, Han JK, Choi BI. Evaluation of hepatic focal lesions using diffusion-weighted MR imaging: comparison of apparent diffusion coefficient and intravoxel incoherent motionderived parameters. J Magn Reson Imaging. 2014; 39:276–285. [PubMed: 23633178]

112. Eckerbom P, Hansell P, Bjerner T, Palm F, Weis J, Liss P. Intravoxel incoherent motion MR imaging of the kidney: pilot study. Adv Exp Med Biol. 2013; 765:55–58. [PubMed: 22879014]

113. Sigmund EE, Cho GY, Kim S, et al. Intravoxel incoherent motion imaging of tumor microenvironment in locally advanced breast cancer. Magn Reson Med. 2011; 65:1437–1447. [PubMed: 21287591]

114. Jensen JH, Helpern JA, Ramani A, Lu H, Kaczynski K. Diffusional kurtosis imaging: the quantification of non-Gaussian water diffusion by means of magnetic resonance imaging. Magn Reson Med. 2005; 53:1432–1440. [PubMed: 15906300]

115. Noda Y, Kanematsu M, Goshima S, et al. Diffusion kurtosis imaging of the pancreas for the assessment of HbA1c levels. J Magn Reson Imaging. 2016; 43:159–165. [PubMed: 26074129]

116. Sun K, Chen X, Chai W, et al. Breast cancer: diffusion kurtosis MR imaging-diagnostic accuracy and correlation with clinical-pathologic factors. Radiology. 2015; 277:46–55. [PubMed: 25938679]

117. Jambor I, Merisaari H, Taimen P, et al. Evaluation of different mathematical models for diffusion-weighted imaging of normal prostate and prostate cancer using high b-values: a repeatability study. Magn Reson Med. 2014 [Epub ahead of print].

118. Bailey DL, Antoch G, Bartenstein P, et al. Combined PET/MR: the real work has just started. Summary Report of the Third International Workshop on PET/MR Imaging; February 17–21, 2014, Tubingen, Germany. Mol Imaging Biol. 2015; 17:297–312. [PubMed: 25672749]

119. Grueneisen J, Schaarschmidt BM, Beiderwellen K, et al. Diagnostic value of diffusion-weighted imaging in simultaneous 18F-FDG PET/MR imaging for whole-body staging of women with pelvic malignancies. J Nucl Med. 2014; 55:1930–1935. [PubMed: 25453042]

120. Metz S, Ganter C, Lorenzen S, et al. Multiparametric MR and PET imaging of intratumoral biological heterogeneity in patients with metastatic lung cancer using voxel-by-voxel analysis. PLoS One. 2015; 10:e0132386. [PubMed: 26186719]
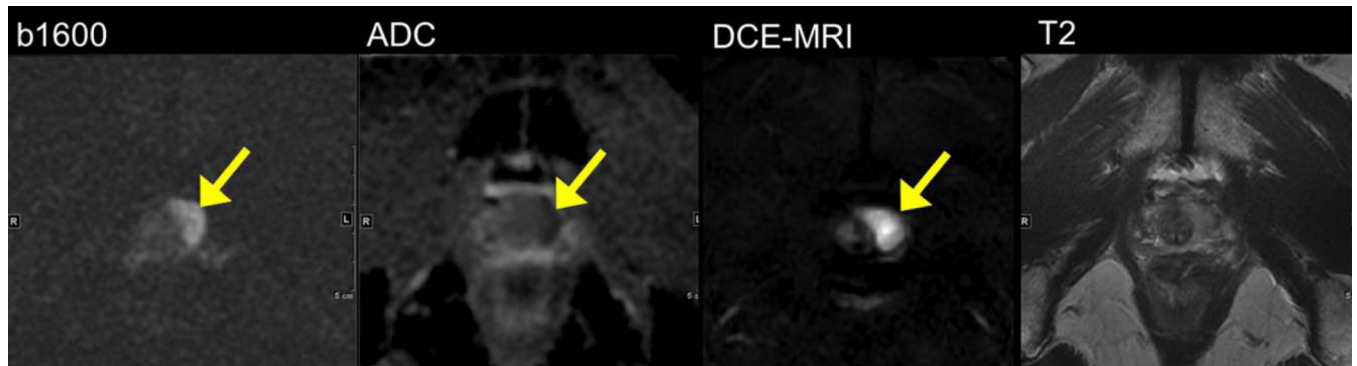
FIGURE 1.

A 68-year-old male with high serum prostate-specific antigen (20 ng/mL) and multiple prior negative prostate biopsies. Reduced FOV DWI at 3.0T (using FOV 24 cm, TR/TE 4000/65, slice thickness 3mm, 160×80) at b1600 demonstrates hyperintense left apex tumor (arrows) with low ADC, and hypervascularity on DCE-MRI. The lesion is isointense on T_2-weighted imaging. The lesion was confirmed to be prostate cancer (Gleason 4 + 3) on targeted ultrasound-guided prostate biopsy.
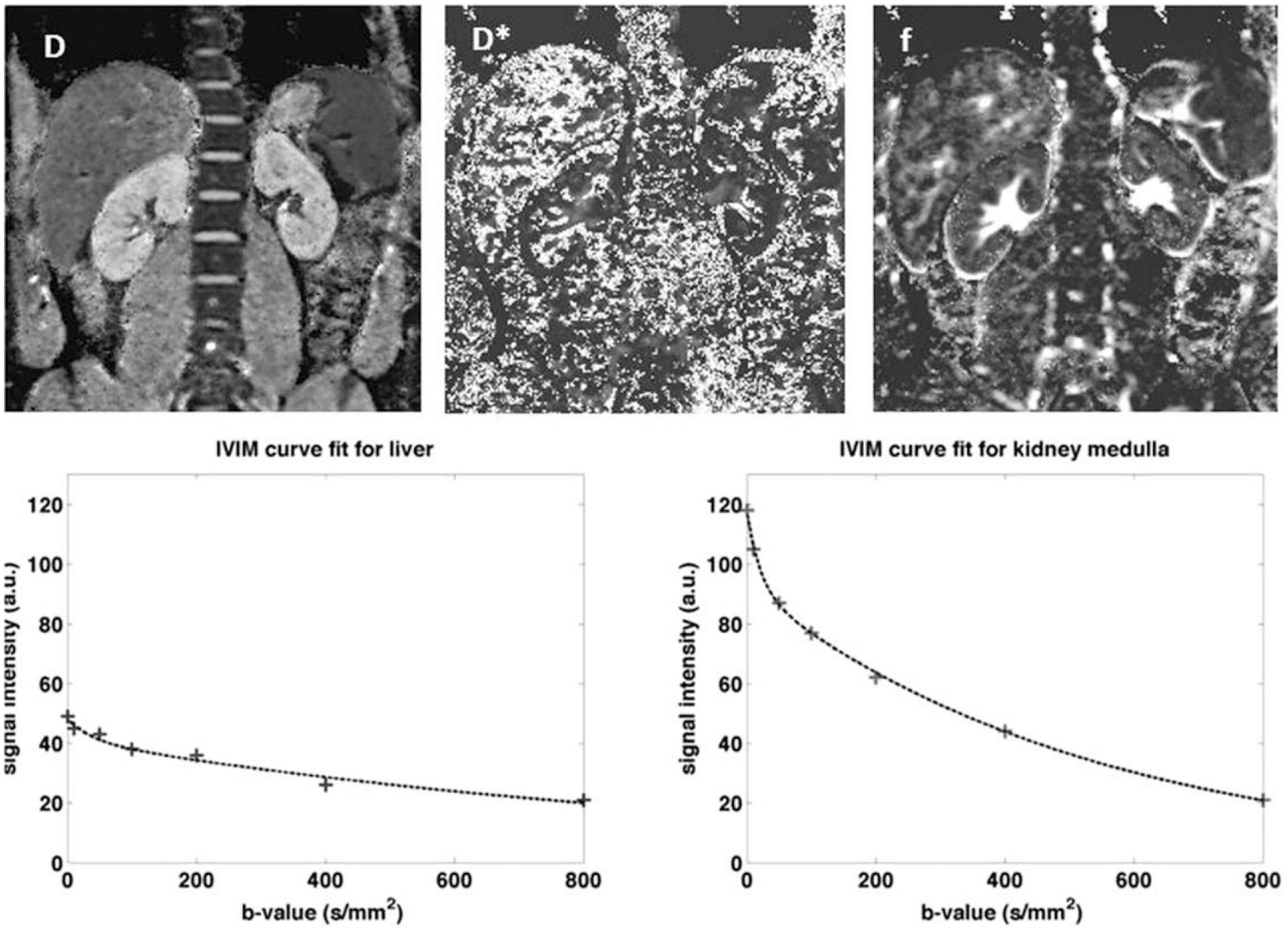
FIGURE 2.
IVIM DWI performed on a 24-year old male volunteer. Coronal DWI performed over the abdomen using seven b-values (0, 25, 50, 100, 200, 400, and 800 s/mm^2) at 1.5T. Diffusion coefficient (D), pseudodiffusion coefficient (D*), and perfusion fraction (f) maps are shown. Note high-quality parametric maps of D and f, while D* map is highly variable. Typical signal attenuation curves of voxel data fitting in the liver and kidneys are shown in the lower row, demonstrating biexponential behavior. IVIM DWI measurements can be made with greater confidence where there is excellent image SNR and in tissues with significant vascular perfusion, as is the case in the liver and kidneys and in many (but not all) types of cancer.
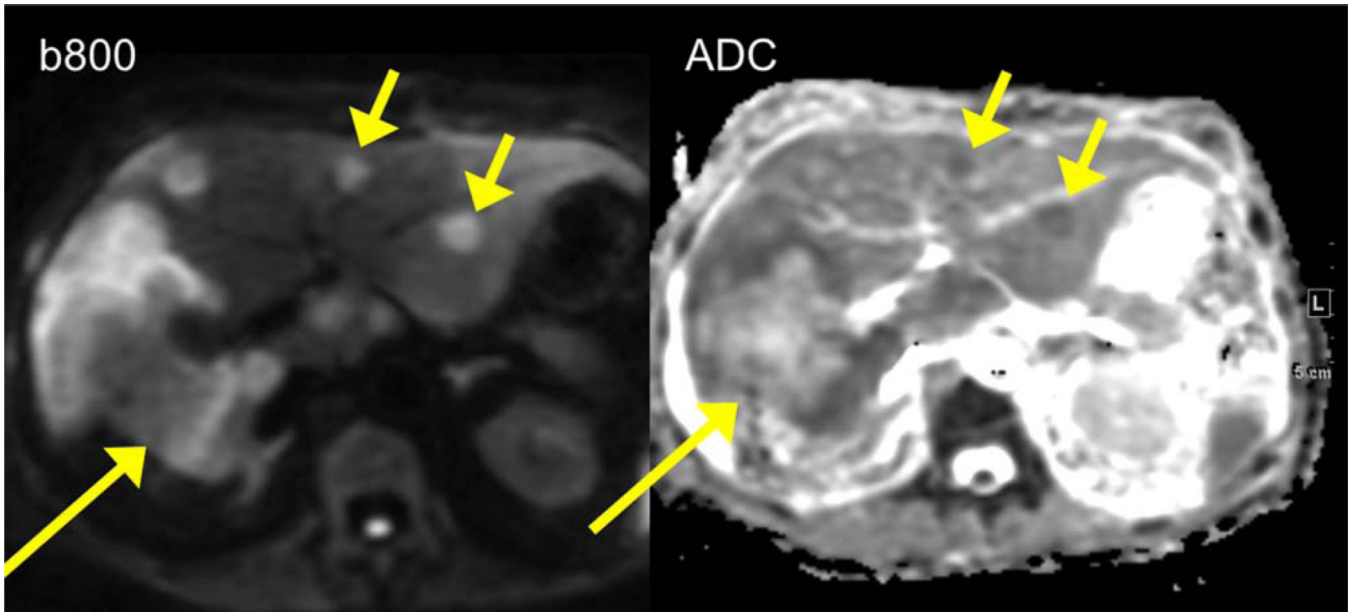
FIGURE 3.
A 51-year-old female with metastatic colon cancer. DW image at b 800 demonstrates an infiltrative tumor (long arrow) in the right hepatic lobe with hyperintense peripheral and hypointense central components, corresponding to low/high ADC (central necrosis and solid peripheral components). There are additional smaller metastatic lesions in the left hepatic lobe with restricted diffusion (short arrows).
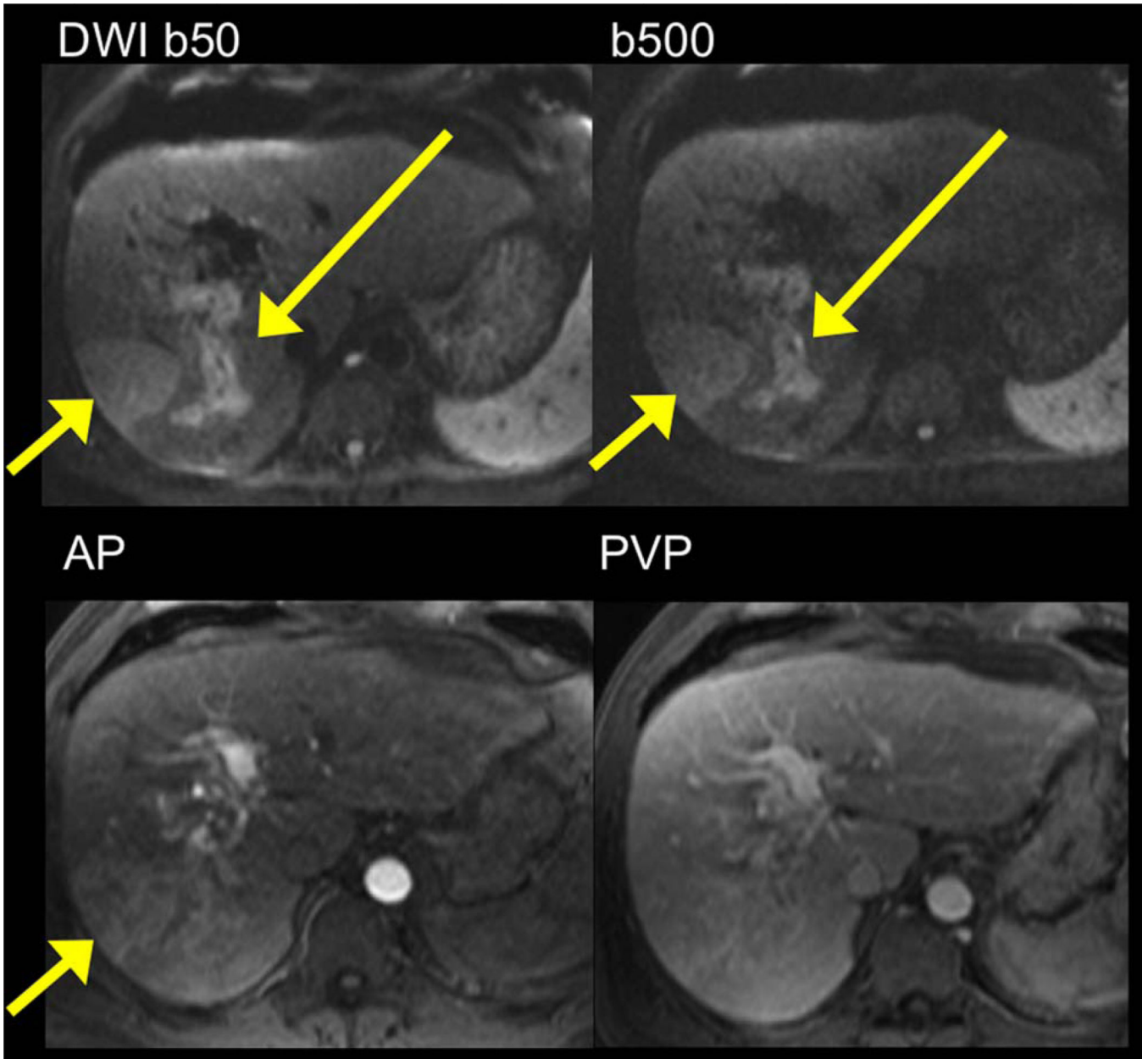
FIGURE 4.

A 69-year-old male with liver cirrhosis secondary to chronic hepatitis C and hepatocellular carcinoma (HCC) with portal vein invasion. DW images at b50 and b500 demonstrate right posterior lobe HCC with restricted diffusion (short arrow) with evidence of tumor thrombus involving the right posterior portal vein (long arrow), better depicted on DWI compared to contrast-enhanced T_1-weighted images at the arterial and portal venous phases (AP and PVP).
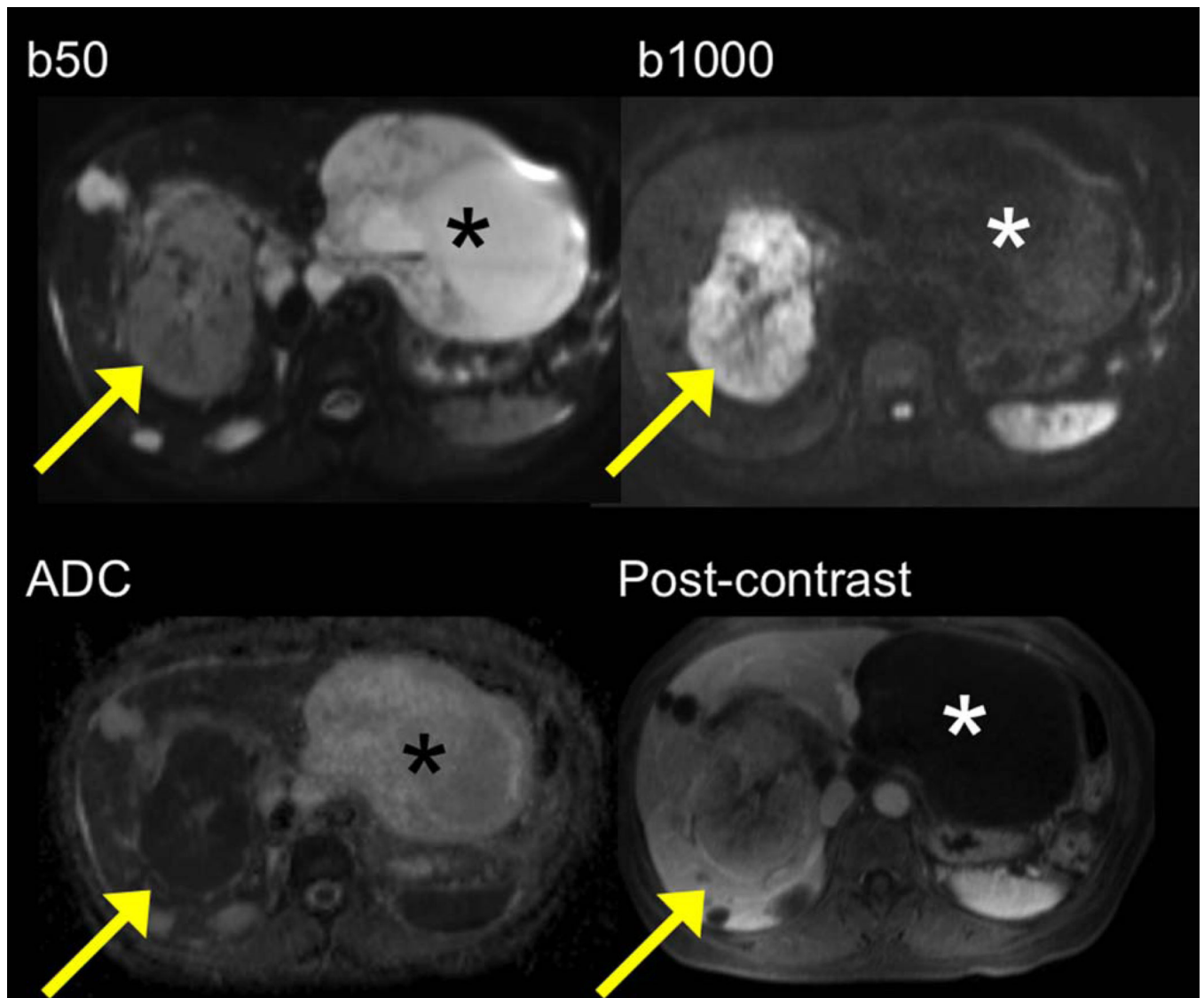
FIGURE 5.
A 60-year-old male with metastatic gastrointestinal stromal tumor. DW images / ADC map demonstrate two large lesions: an intrahepatic lesion (arrow) is mildly hyperintense at b 50 and strongly hyperintense at b 1000 with low ADC (restricted diffusion) compatible with viable tumor. The extrahepatic lesion (asterisk) is strongly hyperintense at b 50, hypointense at b 1000, with high ADC, compatible with necrotic/cystic metastatic lesion. Postcontrast T_1-weighted image confirms DWI findings.

FIGURE 6.
A 60-year-old male with small pancreatic neuroendocrine tumor, better depicted on high b value DWI and fused DWI-T_2 images (arrow). The lesion is not well visible on T_2 HASTE image.
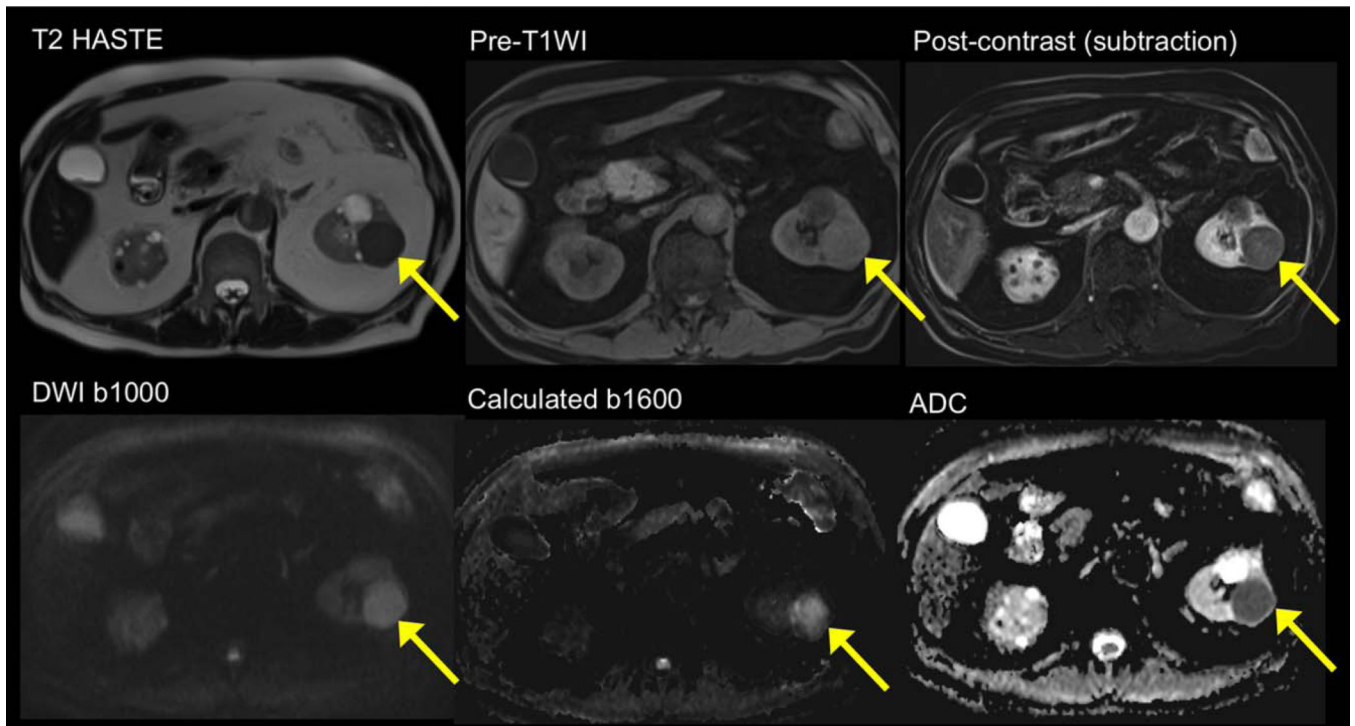
FIGURE 7.
A 60-year-old male with papillary renal cell carcinoma. Standard imaging sequences demonstrate a left renal T_2 hypointense lesion / T_1 hyperintense lesion with evidence of enhancement on subtracted image. The lesion demonstrates restricted diffusion, with high signal on b1000 and on calculated b1600, with low mean ADC (~0.8×10^{-3} mm^2/s).
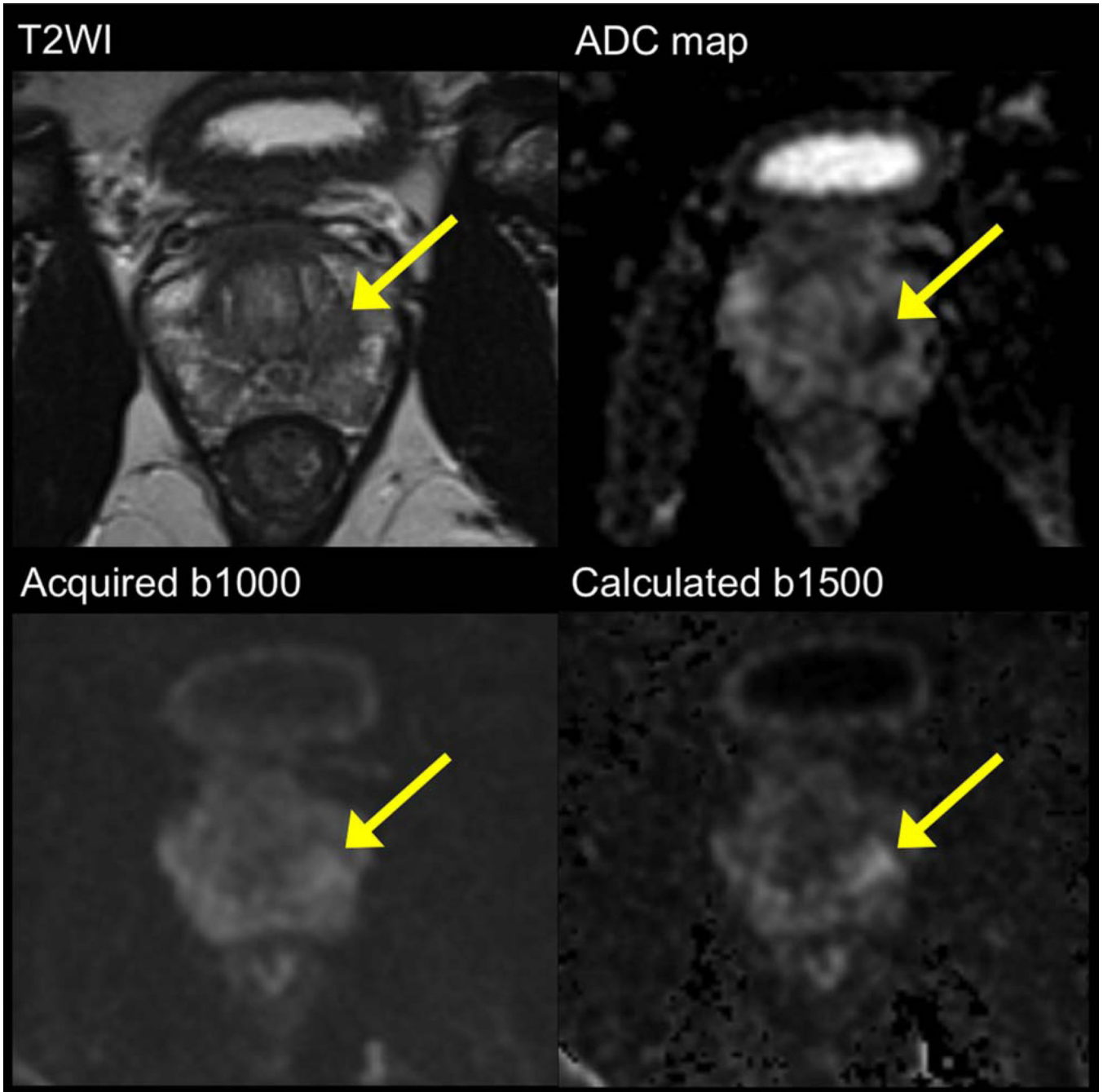
FIGURE 8.

A 55-year-old male with prostate cancer (Gleason score 3 + 4). Left midgland transition zone tumor (arrow) appearing hypointense on T_2WI with low ADC. The tumor is hyperintense on diffusion images, and more conspicuous on calculated b1500 than on acquired b1000 diffusion image, due to incomplete suppression of background benign prostate tissue on b1000 image.
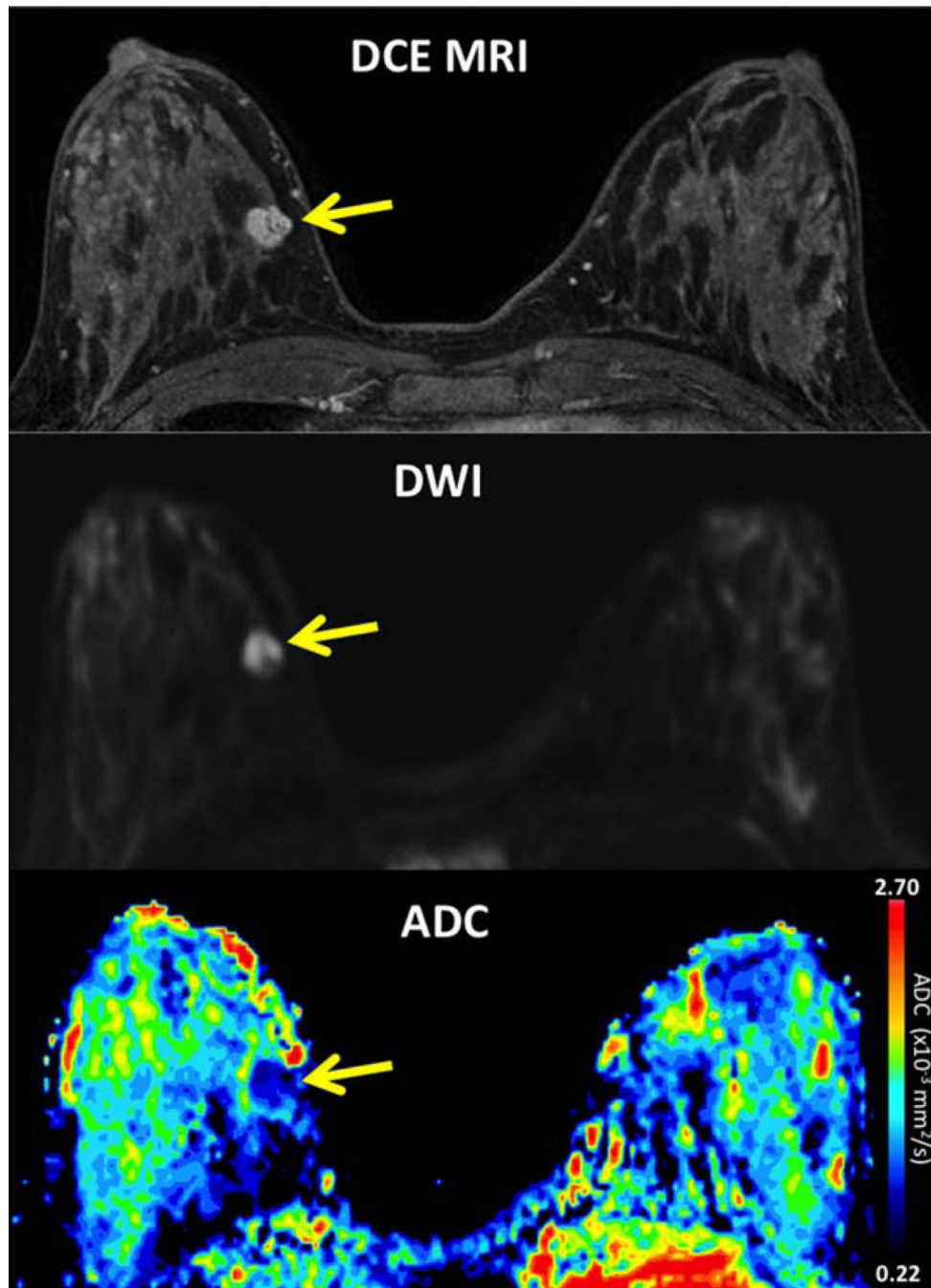
FIGURE 9.
A 31-year-old female with Li-Fraumeni syndrome undergoing breast MRI screening. DCE-MRI demonstrates a mammographically occult mass at 3 o'clock in the right breast (arrow), measuring 11mm with smooth margins and internal septations, rapid enhancement and washout, assessed as BI-RADS category 4. The lesion exhibits restricted diffusion on DWI, with bright signal compared to adjacent parenchyma on b 800 s/mm^2 (arrow) and low ADC of 1.15×10^{-3} mm^2/s. Ultrasound-guided biopsy revealed malignant phyllodes tumor.
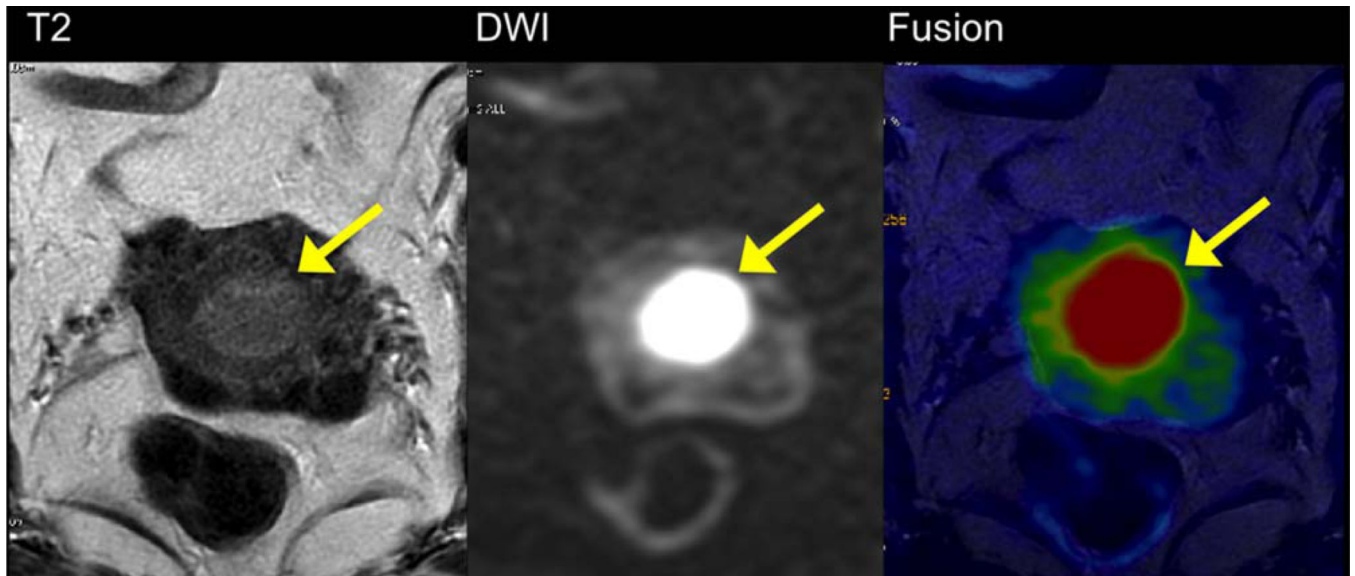
FIGURE 10.
A 70-year-old female with endometrial carcinoma without myometrial infiltration (Stage IA). Comparison of axial oblique T_2WI (A), DWI (B), and fused T_2 and DWI (C). The contrast between the tumor and the myometrium is higher with DWI than with T_2WI with better appreciation of the margins on the fused T_2-DWI image.
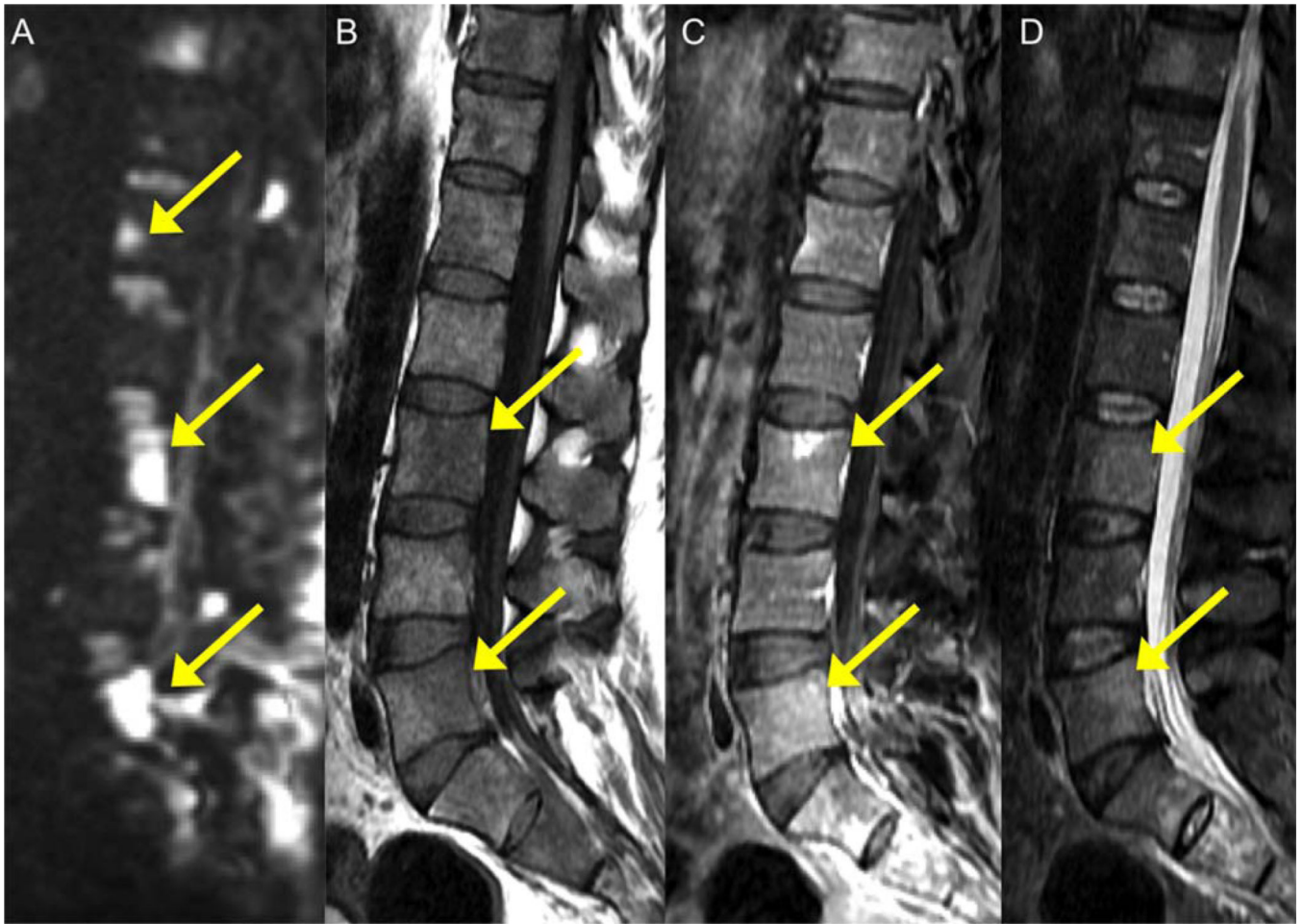
FIGURE 11.
A 59-year-old male with lung cancer and metastatic vertebral lesions. Lesions demonstrate high intensity and high conspicuity on high b value DWI (b1000, arrows) (A) and appear hypointense on T_1WI (B), minimally enhancing on T_1 postcontrast (C), and moderately hyperintense on T_2 WI (D).
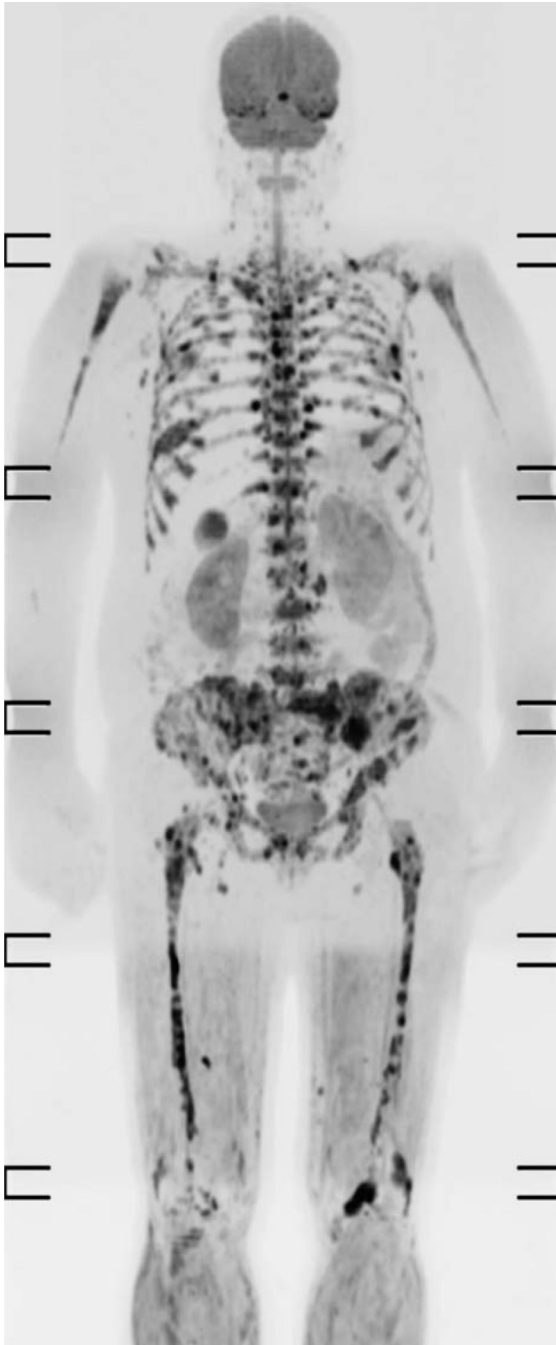
FIGURE 12.
A 60-year-old male with multiple myeloma. Coronal reformatted whole-body DWI image with inverted gray scale contrast for b = 800 s/mm^2 demonstrates diffuse tumor burden in low signal in the bone marrow.
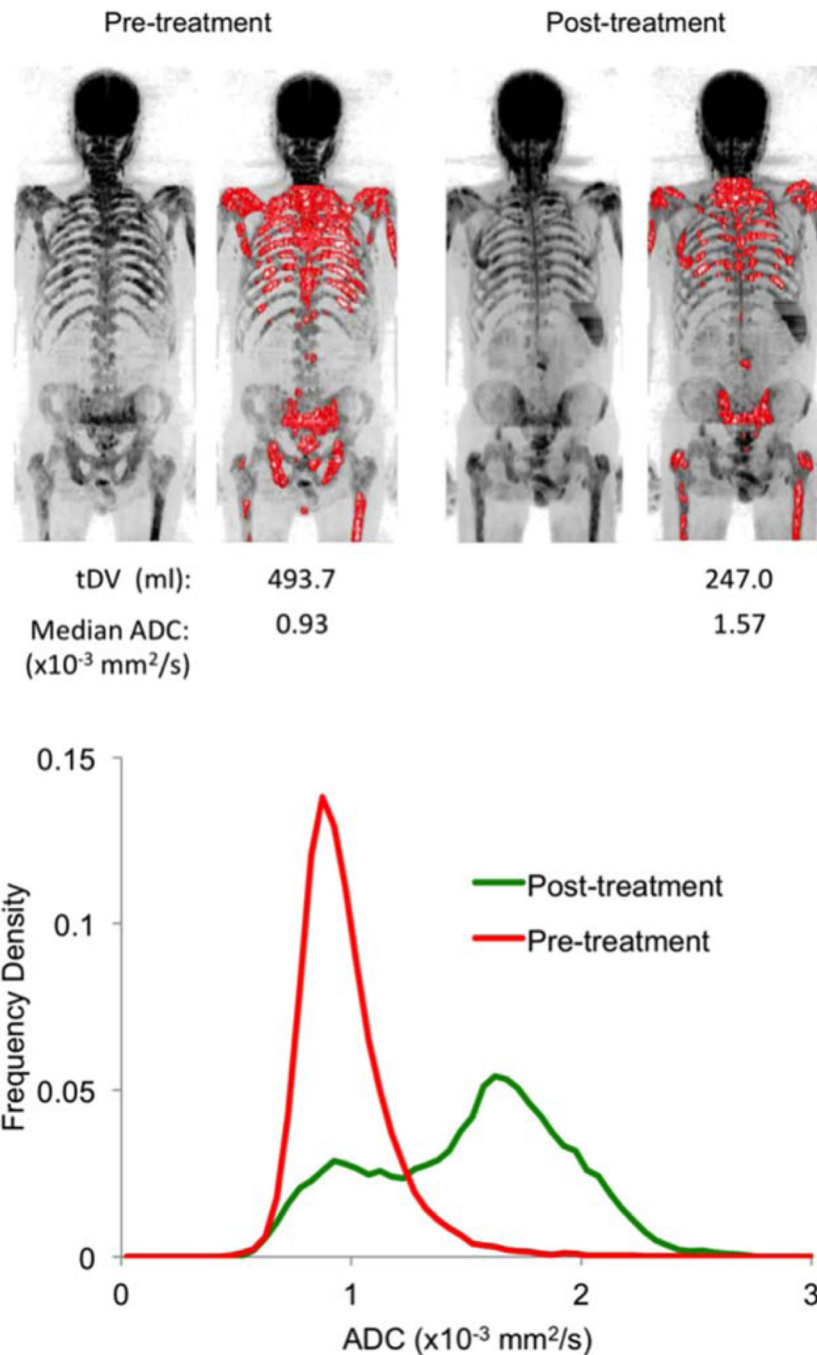
FIGURE 13.
A 65-year-old female with metastatic bone disease from breast cancer. Top row: Pre- and posttreatment inverted gray scale maximum intensity projection b = 900 s/mm^2 images. Disease segmentation (colored red) allows quantification of total disease volume (tDV) before and after treatment. Note reduction in disease volume after chemotherapy. Bottom image: ADC histograms associated with disease volumes pre- and posttreatment shows more than 50% increase in median ADC values after treatment, in keeping with treatment response.
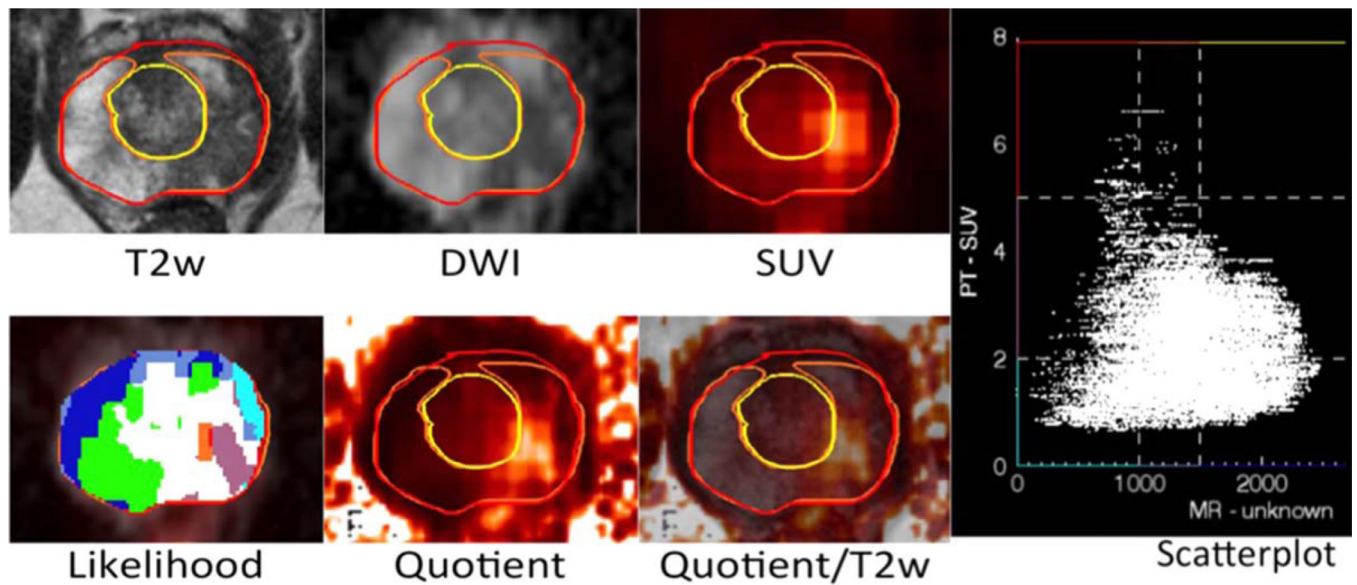
FIGURE 14.

Multimodal multiparametric imaging using Anima M³P (by S.G. Nekolla and S. van Marwick; image courtesy: M. Eiber, D. Vriens). [¹¹C]choline PET/MRI in prostate cancer. By creating a scatterplot of the correlation of SUV (y-axis) and ADC (x-axis), one can define nine different areas ("Likelihood" plot). The most suspicious areas for malignancy are coded in red/orange (highest SUV and lowest ADC). The "Quotient" plot is a map of SUV divided by ADC. The areas with the brightest signal are the most suspicious ones. A biopsy could be targeted to areas with the highest likelihood of malignancy / potentially most aggressive tumor parts.

TABLE 1

Technical Considerations for Acquisition of DWI of the Abdomen and Pelvis

Factor	Suggestion
Underlying pulse sequence	Free-breathing or respiratory-triggered (for abdominal applications) fat-suppressed single-shot echoplanar imaging
TR	3000 msec
TE	Shortest possible (90 msec)
Matrix	At least 128×128 (higher for prostate)
Slice thickness	3–7 mm (3 mm for prostate, matching T2WI)
Parallel imaging reduction factor	2
Number of b-values	At least 2 b-values needed; one or two additional intermediate b-values may be obtained, particularly if performing quantitative ADC measurements
Minimum b-value	<100 s/mm^2
Maximum b-value	800–1000 s/mm^2; further ultra high b-values in range of 1400–2000 sec/mm^2 may be acquired or computed are routinely advised in the prostate
Number of directions	Three directions
SNR considerations	Ensure adequate number of averages and acquisition time to provide sufficient SNR on maximal b-value images
Acquisition plane	Axial (abdomen), axial oblique (prostate), axial or coronal (kidneys), axial or sagittal (female pelvis)
Postprocessing	Inline generation of ADC map using standard monoexponential fit is appropriate for routine clinical applications